American Journal of Pathology, Vol. 163, No. 6, December 2003

Pathogenesis of Ebola Hemorrhagic Fever in Cynomolgus Macaques

Evidence that Dendritic Cells Are Early and Sustained Targets of Infection

Thomas W. Geisbert,* Lisa E. Hensley,* Tom Larsen,* Howard A. Young,† Douglas S. Reed,* Joan B. Geisbert,* Dana P. Scott,* Elliott Kagan,‡ Peter B. Jahrling,* and Kelly J. Davis*

From the United States Army Medical Institute of Infectious Diseases, Fort Detrick; the Laboratory of Experimental Immunology,† Center for Cancer Research, NCI-Frederick, Frederick; and the Uniformed Services University of the Health Sciences,‡ Bethesda, Maryland*

Ebola virus (EBOV) infection causes a severe and fatal hemorrhagic disease that in many ways appears to be similar in humans and nonhuman primates; however, little is known about the development of EBOV hemorrhagic fever. In the present study, 21 cynomolgus monkeys were experimentally infected with EBOV and examined sequentially over a 6-day period to investigate the pathological events of EBOV infection that lead to death. Importantly, dendritic cells in lymphoid tissues were identified as early and sustained targets of EBOV, implicating their important role in the immunosuppression characteristic of EBOV infections. Bystander lymphocyte apoptosis, previously described in end-stage tissues, occurred early in the disease-course in intravascular and extravascular locations. Of note, apoptosis and loss of NK cells was a prominent finding, suggesting the importance of innate immunity in determining the fate of the host. Analysis of peripheral blood mononuclear cell gene expression showed temporal increases in tumor necrosis factor-related apoptosis-inducing ligand and Fas transcripts, revealing a possible mechanism for the observed bystander apoptosis, while up-regulation of NAIP and cIAP2 mRNA suggest that EBOV has evolved additional mechanisms to resist host defenses by inducing protective transcripts in cells that it infects. The sequence of pathogenetic events identified in this study should provide new targets for rational prophylactic and chemotherapeutic interventions. ***(Am J Pathol 2003, 163:2347–2370)***

Among viruses causing hemorrhagic fever (HF), and among emerging infectious diseases with global impact in general, Ebola virus (EBOV) stands out for its impressive lethality. Along with Marburg virus (MBGV), the four species of EBOV (Zaire, Sudan, Reston, Ivory Coast) make up the negative-stranded, enveloped RNA virus family *Filoviridae*. Acute mortality caused by the Zaire species of EBOV is approximately 80% in human outbreaks[1–3] and greater than 90% in monkey models of the genus *Macaca*.[4–7] There is currently no vaccine or therapy for EBOV or MBGV hemorrhagic fever approved for human use. Progress in understanding the origins of the pathophysiologic changes that make EBOV infections of humans so devastating have been slow; a primary reason is the status of filoviruses as biosafety level 4 pathogens necessitating study in high-containment settings.

Animal models that adequately reproduce human EBOV HF are clearly needed to gain further insight into the pathogenesis of this disease. Previous vaccine and drug intervention strategies in rodents, with few exceptions, have failed to predict protection of nonhuman primates against infection with Ebola virus (EBOV). We recently showed that two rodent models of EBOV infection are not ideal for studying human EBOV HF; neither mice nor guinea pigs exhibit the hemorrhagic manifestations that characterize human EBOV infections.[7] Others have also noted differences in coagulopathy between the nonhuman primate and rodent models.[8,9] Furthermore, lymphocyte apoptosis, which is associated with human EBOV HF, was not a prominent feature of EBOV infection in mice or guinea pigs.[10,11] Clinical disease and related pathology in nonhuman primates infected with EBOV appear to more closely resemble features described in human EBOV hemorrhagic fever.[12,13] However, with few exceptions, previous investigations examined naturally infected monkeys or animals killed when moribund, and

Supported by the Medical Chemical/Biological Defense Research Program, U.S. Army Medical Research and Material Command (project number 02–4-4J-081).

Accepted for publication August 26, 2003.

Address reprint requests to Thomas W. Geisbert, USAMRIID, Attn: MCMR-UIV, 1425 Porter Street, Fort Detrick, MD 21702-5011. E-mail: tom.geisbert@amedd.army.mil.

shed little light on the pathogenesis of EBOV infection during times before death. The requirements to demonstrate efficacy of vaccines and/or various chemotherapeutic regimens intended for use in humans demand that the pathogenesis of the disease and correlates of immunity be understood in nonhuman primates.

Several nonhuman primate species have been used to model EBOV (Zaire) HF including African green monkeys (*Chlorocebus aethiops*, formerly *Cercopithecus aethiops*),[4,5,14] cynomolgus macaques (*Macaca fascicularis*),[5,7,15–17] rhesus macaques (*Macaca mulatta*),[4–7,18–20] and hamadryad baboons (*Papio hamadryas*).[21–26] Similar pathological features of EBOV infection have been documented among these species; however, African green monkeys do not present with a macular cutaneous rash, which is a characteristic feature of disease in macaques and baboons.[4–6,15,18–21] Importantly, this rash is also a prominent feature of human disease.[4,14] We focused much of our recent work on cynomolgus macaques, the species most frequently used for filoviral vaccine studies.[7,17] Our cynomolgus monkey model uses a challenge dose and route that reflects a likely laboratory exposure and has been uniformly lethal with animals dying 6 to 7 days after exposure.[7]

Modern virological methods have made it possible to investigate the genetic basis of virulence and to identify the genes and their expression products affecting the severity of the course of disease. While various clinical pathology parameters have provided valuable information regarding filoviral disease, paradigms concerning the intricate pathogenetic mechanisms of EBOV HF require a more thorough understanding of the cells that maintain viral replication and functional changes in infected cells. The aim of this study was to characterize the early stages of EBOV HF in a relevant nonhuman primate model of human disease. Understanding the kinetics of host-pathogen relationships and identification of critical pathogenetic processes are important for the rational development of vaccines and antiviral therapeutics. In the study described here, cynomolgus monkeys were experimentally inoculated with EBOV, and virological and host parameters of infection were longitudinally analyzed.

Materials and Methods

Animals and Inoculations

Healthy, filovirus-seronegative, adult male cynomolgus (*Macaca fascicularis*) macaques ($n = 21$, 4 to 6.5 kg) were used for these studies. Animals were inoculated in the left or right caudal thigh with 1 ml of virus stock that contained 1000 plaque-forming units (PFU) of EBOV (Zaire species). The EBOV used in this study was originally obtained from a fatally infected human from the former Zaire in 1995.[15] Inoculated animals were monitored twice each day for signs of illness. Scheduled necropsies were performed at 1 ($n = 3$), 2 ($n = 3$), 3 ($n = 4$), 4 ($n = 4$), 5 ($n = 4$), and 6 ($n = 3$) days postinfection. Longitudinal blood samples were analyzed by complete blood counts, clinical chemistry, and fluorescence-activated cell sorter analysis of various cell populations (described below). In addition to animals euthanized and exsanguinated for necropsy each day, blood was also collected from 9 of the monkeys at day 1, 12 at day 2, 6 at day 3, and 3 at day 4 postinfection.

Clinical Evaluation

Monkeys were observed twice daily for clinical signs of illness, and signs were recorded on an individual clinical data record maintained for each animal. Each monkey was specifically evaluated for anorexia, diarrhea, nasal exudates, vomiting, conjunctivitis, cutaneous rash, dehydration, central nervous system disturbances, reduced activity, and hemorrhage, using a subjective scoring system.

Hematology

Total white blood cell counts, white blood cell differentials, red blood cell counts, platelet counts, hematocrit values, total hemoglobin, mean cell volume, mean corpuscular volume, and mean corpuscular hemoglobin concentration were determined from blood samples collected in tubes containing ethylene diaminetetraacetic acid (EDTA), using a laser-based hematological Analyzer (Coulter Electronics, Hialeah, FL). The white blood cell differentials were performed manually on Wright-stained blood smears.

Coagulation Tests and Serum Biochemistry

Plasma levels of fibrin degradation products (D-dimers) were quantitated by an enzyme-linked immunosorbent assay (ELISA) according to manufacturer's directions (Asserachrom D-Di; Diagnostica Stago, Inc., Parsippany, NJ). Serum samples were tested for sodium, potassium, chloride, calcium, phosphorus, partial pressure of oxygen (PO_2), partial pressure of carbon dioxide (PCO_2), bicarbonate as total CO_2 content (TCO_2), and pH using an i-STAT Portable Clinical Analyzer (i-STAT Corporation, Princeton, NJ). Concentrations of albumin (ALB), amylase (AMY), alanine aminotransferase (ALT), aspartate aminotransferase (AST), alkaline phosphatase (ALP), γ-glutamyltransferase (GGT), glucose (GLU), cholesterol (CHOL), total protein (TP), total bilirubin (TBIL), urea nitrogen (BUN), and creatinine (Cr) were measured using a Piccolo Point-Of-Care Blood Analyzer (Abaxis, Sunnyvale, CA).

Detection of Endotoxin

Levels of gram-negative bacterial endotoxin in frozen plasma samples were measured with a commercially available chromogenic limulus amebocyte assay (Bio-Whittaker, Walkersville, MD). The absorbance of each microplate well was read at 405 to 410 nm, and endotoxin concentrations were calculated by linear regression. To control for nonspecific background, baseline absorbance levels were collected immediately after addition of chromagen (before development) and subtracted from

the absorbance measured after development. This corrected value was then used for the calculation of endotoxin concentration. The virus inoculum used in this study was assayed and shown to be free of endotoxin (< 0.1 EU/ml).

Cytokine/Chemokine and Nitrate Production

Cytokine/chemokine levels in monkey sera/plasma were assayed using commercially available ELISA kits according to manufacturer's directions. Cytokines/chemokines assayed included monkey interleukin (IL)-2, IL-4, IL-10, IL-12, interferon (IFN)-γ, and tumor necrosis factor (TNF)-α (BioSource International, Inc., Camarillo, CA). ELISAs for human proteins known to be compatible with cynomolgus macaques included IL-6, IFN-α, IFN-β, MIP-1α, and MIP-1β (BioSource); and human IL-1β, IL-8, IL-18, and MCP-1 (R&D Systems, Minneapolis, MN). Nitrate levels were determined using a colorimetric assay according to manufacturer's directions (R&D Systems).

Necropsy

A complete necropsy was performed on all animals. Tissue samples of all major organs were collected from each monkey for histopathological, immunohistochemical, and *in situ* hybridization examination and were immersion-fixed in 10% neutral-buffered formalin. Select tissues for ultrastructural examination were immersion-fixed in 4% formaldehyde plus 1% glutaraldehyde in 0.1 mol/L Millonig's phosphate buffer for transmission electron microscopy (TEM) or 2% formaldehyde plus 0.1% glutaraldehyde in the Millonig's buffer for immunoelectron microscopy.

Histology

Formalin-fixed tissues for histology, immunohistochemistry, and *in situ* hybridization were processed and embedded in paraffin according to conventional methods.[27] Histology sections were cut at 5 to 6 μm on a rotary microtome, mounted on glass slides, and stained with hemotoxylin and eosin. Replicate sections of all tissues were mounted on positively charged glass slides (Superfrost Plus; Fisher Scientific, Pittsburgh, PA) and immunohistochemically stained for detection of viral antigen by an immunoperoxidase method according to kit procedures (Envision System; DAKO Corporation, Carpinteria, CA), or by a fluorescence-based method.

Immunohistochemistry

Immunoenzymatic Methodology

Sections were deparaffinized and rehydrated through a series of graded ethanols, pretreated with ready-to-use Proteinase K (DAKO) for 6 minutes at room temperature, and blocked with Protein Block Serum-Free (DAKO) for 20 minutes before exposure to antibody. Tissue sections were incubated with primary antibody overnight a 4°C using an anti-EBOV rabbit polyclonal (kindly provided by Cindy Rossi) (1:500) or an equal mixture of mouse monoclonal antibodies to EBOV GP and VP40 (1:5000).[6] An alkaline phosphatase-labeled polymer (DAKO Envision System, alkaline phosphatase) was added for 30 minutes and color development was achieved by exposing tissue to the substrate 6-bromo-2-hydroxyl-3-naphtholic acid (Histomark Red; Kirkegaard and Perry, Gaithersburg, MD) for 50 minutes in the dark. Sections were counterstained with hematoxylin. Negative controls included replicate sections exposed to anti-Marburg virus antibodies and unexposed cynomolgus monkey tissue; archived EBOV-infected cynomolgus tissue served as positive controls.

Immunofluorescence Methodology

Tissue sections were deparaffinized, rehydrated, and incubated in 20 μg/ml of proteinase K for 30 minutes at room temperature. Sections were subsequently rinsed, placed in normal goat serum for 20 minutes and transferred to a mixture of the anti-EBOV monoclonal antibodies as described above for 30 minutes at room temperature. After incubation, sections were rinsed and stained with goat anti-mouse Alexa 594 (Molecular Probes, Eugene, OR), incubated with a pan T-cell marker, CD3 (DAKO) for 30 minutes at room temperature, rinsed, and incubated in goat anti-mouse Alexa 488 (Molecular Probes).

For co-localization of macrophage and/or dendritic cell markers and EBOV antigens, two different techniques were performed. Briefly, deparaffinized tissue sections were pretreated with proteinase K (20 μg/ml) for 30 minutes at room temperature and incubated in normal goat serum for 20 minutes. Sections were then incubated in either a macrophage marker (Ab-1, Oncogene Research Products, San Diego, CA), or a marker for dendritic cells (DC-SIGN, kindly provided by Dr. Vineet KewalRamani, NCI-Frederick), for 30 minutes at room temperature. After incubation, sections were placed in goat anti-mouse Alexa 594 (Molecular Probes) for 30 minutes at room temperature and rinsed. Sections were transferred to a blocking solution consisting of a cocktail of mouse IgGs and irrelevant mouse anti-Marburg virus antibodies, and incubated for 20 minutes at room temperature. The excess blocking cocktail was removed and sections were incubated in a fluorescein isothiocyanate (FITC)-conjugated EBOV for 30 minutes at room temperature. The FITC-conjugated anti-EBOV pool was produced by diluting the purified, concentrated anti-EBOV murine monoclonal antibodies (described above) to 1 mg/ml and dialyzing overnight at 4°C in 0.1 mol/L sodium bicarbonate buffer (pH 8.5). The antibodies were recovered and mixed with FITC on celite (σ-Aldrich, St. Louis, MO) and incubated, rotating, for 2 hours at room temperature. FITC-conjugated antibodies were then separated from unbound FITC by passage over a Sephadex G-25 (Amersham Biosciences, Piscataway, NJ) column. To increase the sensitivity of the staining, sections were incubated in an anti-FITC Alexa 488 (Molecular Probes) for 30 minutes at room temperature. After rinsing in PBS, sections were mounted in an aqueous mounting medium containing 4′,6′-diamidino-2-phenylindole (DAPI) (Vector

Laboratories, Burlingame, CA) and examined with a Nikon E600 fluorescence microscope (Nikon Instech Co., Ltd., Kanagawa, Japan).

To confirm co-localization patterns, double stains were also performed using a rabbit anti-EBOV polyclonal antibody. Briefly, following proteinase K digestion, blocking in normal goat serum, and incubation in either the anti-macrophage marker or DC-SIGN antibody, sections were incubated in goat anti-mouse Alexa 488 for 30 minutes at room temperature. Sections were rinsed, incubated in rabbit anti-EBOV antibody for 30 minutes at room temperature, rinsed, and incubated in goat anti-rabbit Alexa 594 (Molecular Probes). After rinsing in PBS, sections were mounted in an aqueous mounting medium containing DAPI (Vector Laboratories) and examined with a Nikon E600 fluorescence microscope (Nikon Instech Co.) and/or a Bio-Rad Radiance2000MP confocal microscope (Bio-Rad, Hercules, CA).

In Situ *Hybridization*

EBOV GP and VP40 RNA were localized in tissues using digoxigenin-labeled DNA probes. Probe constructs were plasmids (pCR2.1; Invitrogen, Carlsbad, CA) containing complementary DNA sequences for EBOV GP or VP40. Probes were labeled by nick translation with digoxigenin-11-UTP (Boehringer Mannheim, Indianapolis, IN) following the manufacturer's recommendations. Before hybridization, tissue sections were incubated with 40 μg/ml of nuclease-free proteinase K (Boehringer Mannheim) in Tris-buffered saline (pH 7.6) for 30 minutes at 37°C. For hybridization, probes were denatured at 95°C for 5 minutes, placed on ice, and then applied to tissue sections and incubated overnight at 42°C. After hybridization, sections were washed in buffer, and incubated in alkaline phophatase-conjugated, antidigoxigenin antibody (Boehringer Mannheim), diluted 1:600, for 1 hour at 37°C. Sections were washed and the color was developed with 5-bromo-4-chloro-3-indolyl phosphate (NBT/BCIP, Life Technologies, Gaithersburg, MD) as the substrate and nitro blue tetrazolium salt (NBT) as the chromagen for 1 hour at 37°C. Sections were counterstained with nuclear fast red (Vector Laboratories). Tissue sections incubated in the pCR2.1 plasmid lacking the EBOV gene inserts served as negative controls.

TUNEL Staining

Spleen and various lymph nodes were evaluated for apoptosis using both a chromagen-based *in situ* terminal deoxynucleotidyl transferase mediated deoxyuridine triphosphate nick-end labeling (TUNEL) assay (In Situ Cell Death Detection Kit, Roche, Indianapolis, IN) or a fluorescence-based TUNEL assay (ApopTag assay; Intergen, Purchase, NY) as previously described.[28] A pan B-cell marker, CD20 (DAKO); a pan T-cell marker, CD3 (DAKO); a plasma cell marker, NCL-PC (Vector Laboratories); and a macrophage marker, Ab-1 (Oncogene Research Products) were used to aid in identifying architectural landmarks within the lymphoid tissues and in identifying apoptotic cell types.[28]

Electron Microscopy

Paraformaldehyde/glutaraldehyde-fixed tissues and peripheral blood mononuclear cells for transmission electron microscopy were postfixed in 1% osmium tetroxide in 0.1 mol/L Millonig's phosphate buffer, rinsed, stained with 0.5% uranyl acetate in ethanol, dehydrated in graded ethanol and propylene oxide, and embedded in Poly/Bed 812 resin (Polysciences, Warrington, PA). Areas to be examined by electron microscopy were selected from 1-μm sections stained with toluidine blue. Ultrathin sections were cut, placed on 200-mesh copper electron microscopy grids, stained with uranyl acetate and lead citrate, and examined using a JEOL 1200 EX transmission electron microscope (JEOL Ltd., Peabody, MA) at 80 kV.

Post-embedding immunoelectron microscopy was performed on portions of aldehyde-fixed inguinal lymph node and spleen, embedded in LR White resin (Polysciences). Briefly, ultrathin sections were floated on drops of 4% normal goat serum in 0.1% bovine serum albumin plus 0.05% Tween 20 in 0.2 mol/L Tris (BTT), then incubated with the primary antibodies (either the DC-SIGN marker for dendritic cells described above or irrelevant isotype control). Sections were then incubated with goat-anti-mouse IgG conjugated to 10 nm colloidal gold, rinsed, stained with uranyl acetate and lead citrate and examined with a JEOL 1200 EX transmission electron microscope (JEOL) at 80 kV.

Virus Isolation from Plasma and Tissues

Infectious virus in EDTA plasma was assayed by counting plaques on Vero cells maintained as monolayers in 6-well plates under agarose, as previously described.[29] Portions of liver, spleen, lung, kidney, adrenal gland, pancreas, heart, testis, brain, femoral bone marrow, and mandibular, axillary, and left and right inguinal lymph nodes were aseptically collected during necropsy and stored at −70°C until assayed for virus. After thawing, tissues were weighed and ground by mortar and pestle with alundum in 5 ml of Eagle's minimal essential medium (EMEM) with Earl's salts with 10% fetal calf serum. Tissue homogenates were centrifuged at 10,000 × *g* for 15 minutes and viral titers were determined as detailed above.

RNase Protection Assays

Peripheral blood mononuclear cells were separated from EDTA-treated peripheral blood collected from monkeys before and after exposure to EBOV by centrifugation on Histopaque (σ-Aldrich) at 250 × *g* for 30 minutes. Cells at the interface were harvested, washed in RPMI 1640, and treated with TriZol. The Multiprobe RNase Protection

Table 1. Clinical Findings in Cynomolgus Monkeys Infected with Ebola Virus

Days postinfection	Fever	Rash	Bleeding	Anorexia	Dehydration	Recumbency
0	0/21	0/21	0/21	0/21	0/21	0/21
1	0/12	0/21	0/21	0/21	0/12	0/21
2	0/15	1/18	0/18	0/18	0/15	0/18
3	3/10	3/15	0/15	0/15	0/10	0/15
4	6/7	4/11	0/11	2/11	2/7	0/11
5	7/7	7/7	0/7	6/7	2/7	0/7
6	0/2	2/2	2/2	2/2	2/2	2/2

Data are presented as the number of animals in which a clinical finding was observed/total number of animals examined. Fever and dehydration were evaluated in animals anesthetized for phlebotomy and/or physical examination. Rash, bleeding, anorexia, and recumbency were monitored in all remaining animals at the specified time point.

Assay was performed according to the manufacturer's directions (Pharmingen, San Diego, CA) with the minor modifications as previously described.[30]

Flow Cytometric Analysis of PBMC

The following monoclonal antibodies were obtained from Pharmingen and used in this study: anti-human CD3-FITC (SP34), CD4-PE (RPA-T4), CD8-APC (RPA-T8). Peripheral blood mononuclear cells (PBMC) isolated from EBOV-infected macaques were washed in RPMI containing 10% fetal calf serum and then frozen at −70°C in media containing 10% dimethyl sulfoxide. For flow cytometry analysis, PBMC were thawed and washed twice with PBS (pH 7.4), containing 0.5% bovine serum albumin (BSA) and 0.1% sodium azide (PBA). The cells were resuspended with 100 μl of diluted monoclonal antibody specific for surface antigens followed by incubation at 4°C for 20 minutes. Cells were washed twice with PBA, fixed by resuspension in 3% paraformaldehyde buffer and stored at 4°C overnight. Flow cytometric analysis of the samples was then conducted using a FACSCalibur (Becton Dickinson, San Jose, CA). Data were analyzed using WinMDI software (The Scripps Research Institute, La Jolla, CA).

Results

Clinical Illness

The principal clinical findings are presented in Table 1. Clinical illness was unremarkable until day 3 when 3 of 10 (3/10) animals given physical examinations had fevers (defined as temperature over 102°F), with temperatures ranging from 103.3°F to 104.1°F; one of these animals and two afebrile animals had cutaneous rashes involving the axilla and/or groin. By day 4, 6 of 7 monkeys given physical examinations were febrile, with temperatures ranging from 103.2°F to 104.5°F; three of these animals had macular cutaneous rashes on the arms (Figure 1A) and groins, and on two of these animals, the rash also involved the thorax, proximal limbs, and face, particularly on the periorbital area and forehead. Mild dehydration (approximately 5% as evaluated subjectively by skin-fold retraction) and anorexia were noted in two animals and diarrhea was seen in a single animal. By day 5, all seven remaining animals were febrile and had characteristic macular cutaneous rashes (Figure 1B); 6 of 7 animals were anorexic, two showed 10% dehydration, four remained sitting in a hunched-over position favoring the abdomen with either of their arms; all showed signs of moderate to severe depression. At day 6, one animal,

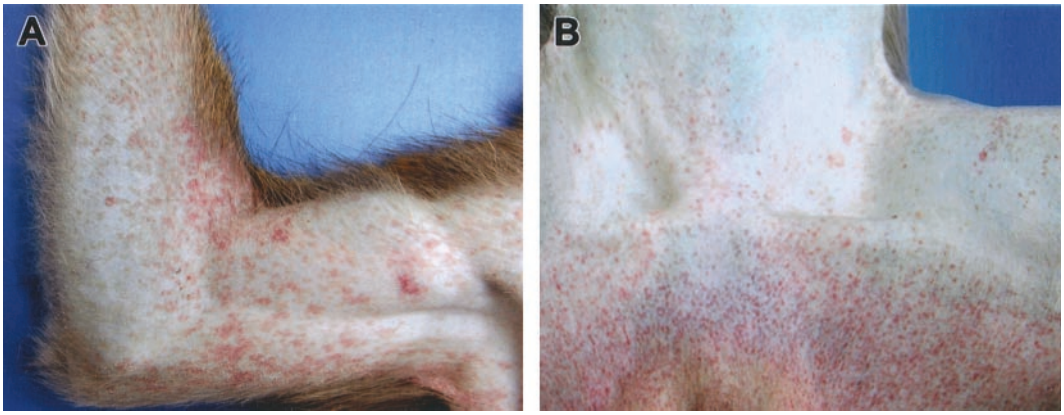

Figure 1. Representative cutaneous rashes from cynomolgus monkeys experimentally infected with EBOV-Zaire. **A:** Characteristic petechial rash of the right arm at day 4. **B:** Petechial rash of the inguinal region at day 5.

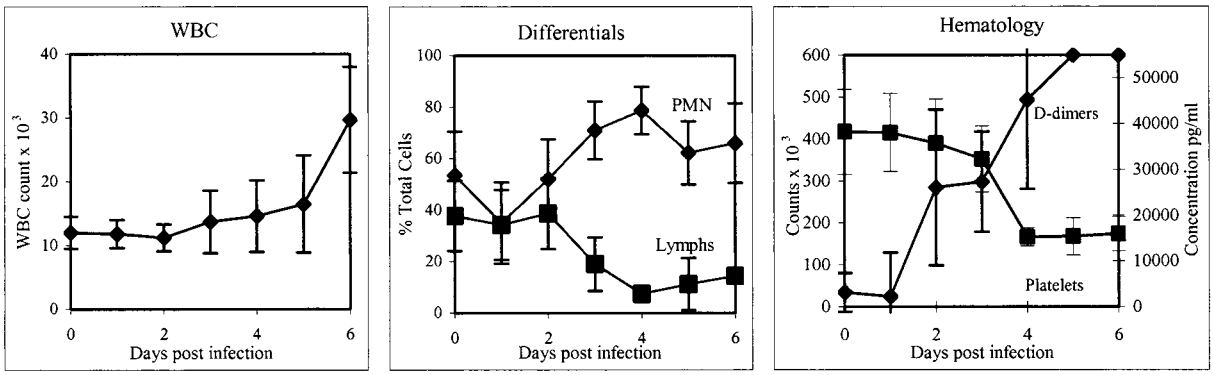

Figure 2. Hematology values after infection of cynomolgus monkeys with EBOV-Zaire. Total white blood cell counts (**left**) and differential white blood cell counts (**center**) show a developing leukocytosis due to an increased neutrophilia. Also, note concomitant lymphopenia. PMN, polymorphonuclear neutrophils; Lymphs, lymphocytes. **Right:** Development of thrombocytopenia and D-dimers.

which had been monitored late the previous evening, was found dead early in the morning. The remaining two animals were recumbent and had depressed body temperatures. Both animals had macular cutaneous rashes; one of these animals bled from the nares while the other animal bled from the rectum.

Hematology, Flow Cytometry, and Clinical Chemistry

Total and differential white blood cell counts revealed developing leukocytosis due to an increased neutrophilia (Figure 2). By day 6, the mean white blood cell counts were 2.5 times the baseline values. Neutrophils ranged from approximately 58% of the leukocyte population on day 1 to 79% on day 4 (an approximate 1.4-fold increase), while monocytes declined from approximately 4% on day 1 to 0.75% on day 5. There was a concomitant lymphopenia as lymphocytes dropped from approximately 33% of the leukocyte population on day 1 to less than 9% on day 4, and then appeared to slightly rebound to just less than 15% on day 6 (Figure 2). Thrombocytopenia developed as platelets declined from a preinfection mean of $412 \times 10^3/mm^3$ to $174 \times 10^3/mm^3$ on day 6 (Figure 2). A slight decline in platelets began on day 2 with a significant drop occurring between days 3 and 4. Development of fibrin degradation products (D-dimers) showed rapid increases of 45-fold by day 4 and 55-fold by day 5 (Figure 2). Hemoglobin, hematocrit, and erythrocyte counts dropped between preinfection levels and day 6 with the most notable drop occurring between days 4 and 5. Nucleated red blood cells were detected in peripheral blood smears of all animals at days 5 and 6. Döhle bodies were seen in neutrophils of all animals by day 4, and marked increases in immature neutrophils (band cells) were also noted in all monkeys by day 4.

Flow cytometry was used on PBMC to better understand changes in these cells during the course of lethal EBOV infection. Depletion of CD4 and CD8 lymphocytes developed as the disease progressed while the number of circulating B lymphocytes remained constant. Separation of the CD8 subset into NK cells and T lymphocytes showed a dramatic decline in the NK population with nearly 75% decrease in numbers by day 4 (Figure 3). This pattern of NK and CD8 lymphocyte depletion was consistent for all macaque samples examined during this study (D.S. Reed, in preparation). For example, at day 2 a 14% reduction was observed in levels of both NK cells ($n = 9$) and CD8 lymphocytes ($n = 9$). By day 3, a 55% reduction was seen in levels of NK cells ($n = 6$) while a 45% reduction was noted in levels of CD8 lymphocytes ($n = 6$). Examination of other surface antigens (CD69, CD25, CD44) suggested that little if any T or B lymphocyte activation occurred after EBOV exposure (D.S. Reed, in preparation).

Early serum enzyme levels were unremarkable, but all were elevated during the late stages of disease (Figure 4). On day 6, AST rose sharply (range, 1287 to 1671 IU/L) as did ALT (range, 237 to 511 IU/L). AP levels were increased nearly fourfold over baseline values, while GGT levels increased approximately 2.5-fold over baseline. BUN levels remained generally within normal limits through day 4, after which, on day 5 and 6, there were marked elevations (2.5- and 5.5-fold over baseline, respectively). Serum creatinine levels increased nearly sixfold over baseline by day 6. Total serum proteins did not fluctuate during the course of infection; however, decreases in serum albumin levels were seen by day 4, indicating a loss of only small molecular weight proteins.

Necropsy Findings

Necropsy findings were unremarkable in the animals euthanized at 24 and 48 hours. By day 3 and continuing through day 6, inguinal lymph nodes of all EBOV-infected monkeys were enlarged (1.5 to 3 times normal size) and reddened. Similar changes (lymphadenopathy) of the axillary lymph nodes appeared by day 3 in 3 of 4 (3/4) animals necropsied and were a consistent finding through day 6 (Figure 5A). Lymphadenopathy of mandibular and mesenteric lymph nodes was seen in 1 of 4 animals by day 4 and was present in all animals thereafter. The liver was slightly enlarged with rounded friable capsular borders and had a reticulated pattern visible

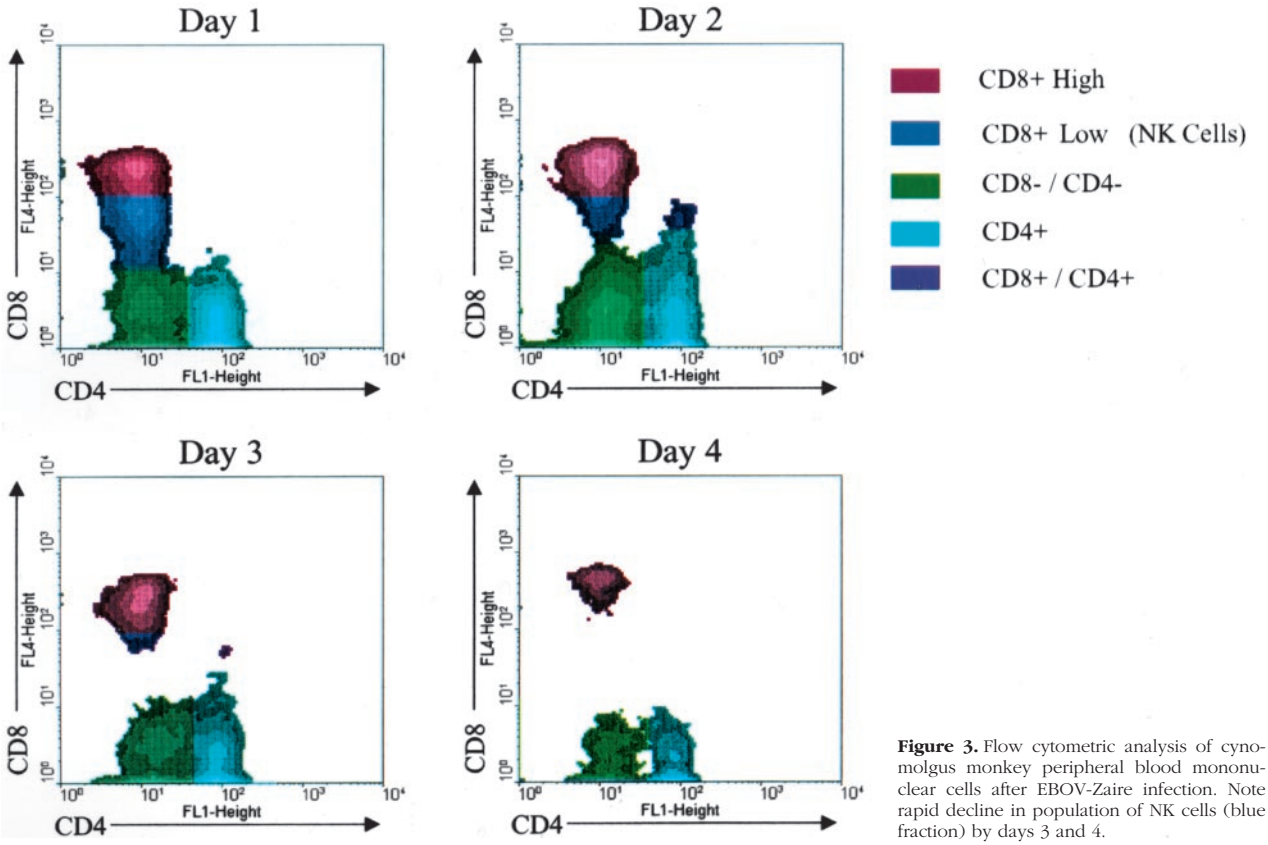

Figure 3. Flow cytometric analysis of cynomolgus monkey peripheral blood mononuclear cells after EBOV-Zaire infection. Note rapid decline in population of NK cells (blue fraction) by days 3 and 4.

from the capsular surface at days 4 through 6. Other findings at day 4 included bilateral enlargement (2 times normal size) and reddening of the tonsils (2 of 4), and mild congestion of the small intestine (1 of 4). The presence of gross lesions increased dramatically between days 4 and 5. Findings at days 5 and 6 were similar and included urinary bladder petechiae (4 of 7) (Figure 5B), a sharply demarcated zone of congestion at the junction of the pylorus and the duodenum (5 of 7) (Figure 5, C and D), a reddening of the ileocecal valve interpreted as congestion in the gut-associated lymphoid tissue (GALT) (6 of 7) (Figure 5, E and F), congestion of the proximal colon GALT (3 of 7), congestion of adrenal glands (6 of 7), petechiae and congestion of the rectum (1 of 7), bilateral testicular petechiae and ecchymoses (3 of 7), hemorrhage of gums (1 of 7), presence of petechiae on gums and buccal membranes (1 of 7), bilateral reddening and enlargement of tonsils (2 of 7), ulceration of glandular mucosa of stomach (1 of 7), and multifocal epicardial petechiae (1 of 7).

Virus Titers in Blood and Tissues

Onset of plasma viremia was rapid, occurred within 3 days, and ranged from 1.4 to 4.2 $\log_{10}$ pfu/ml (mean,

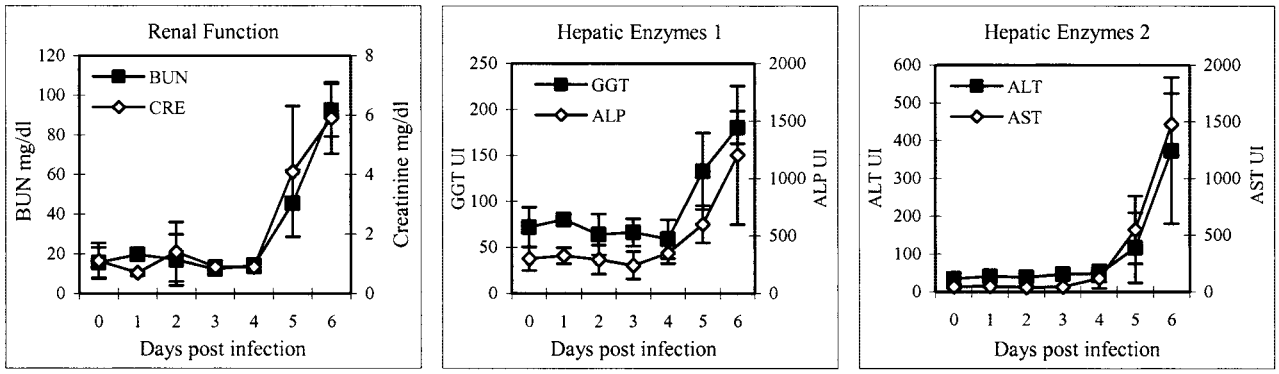

Figure 4. Clinical chemistry values after infection of cynomolgus monkeys with EBOV-Zaire showing elevated levels of serum enzymes primarily at the late stages of disease (days 5 and 6). **Left:** Blood urea nitrogen (BUN) and creatinine. **Center:** γ-glutamyl transferase (GGT) and ALP (alkaline phosphatase). **Right:** Alanine aminotransferase (ALT) and aspartate aminotransferase (AST).

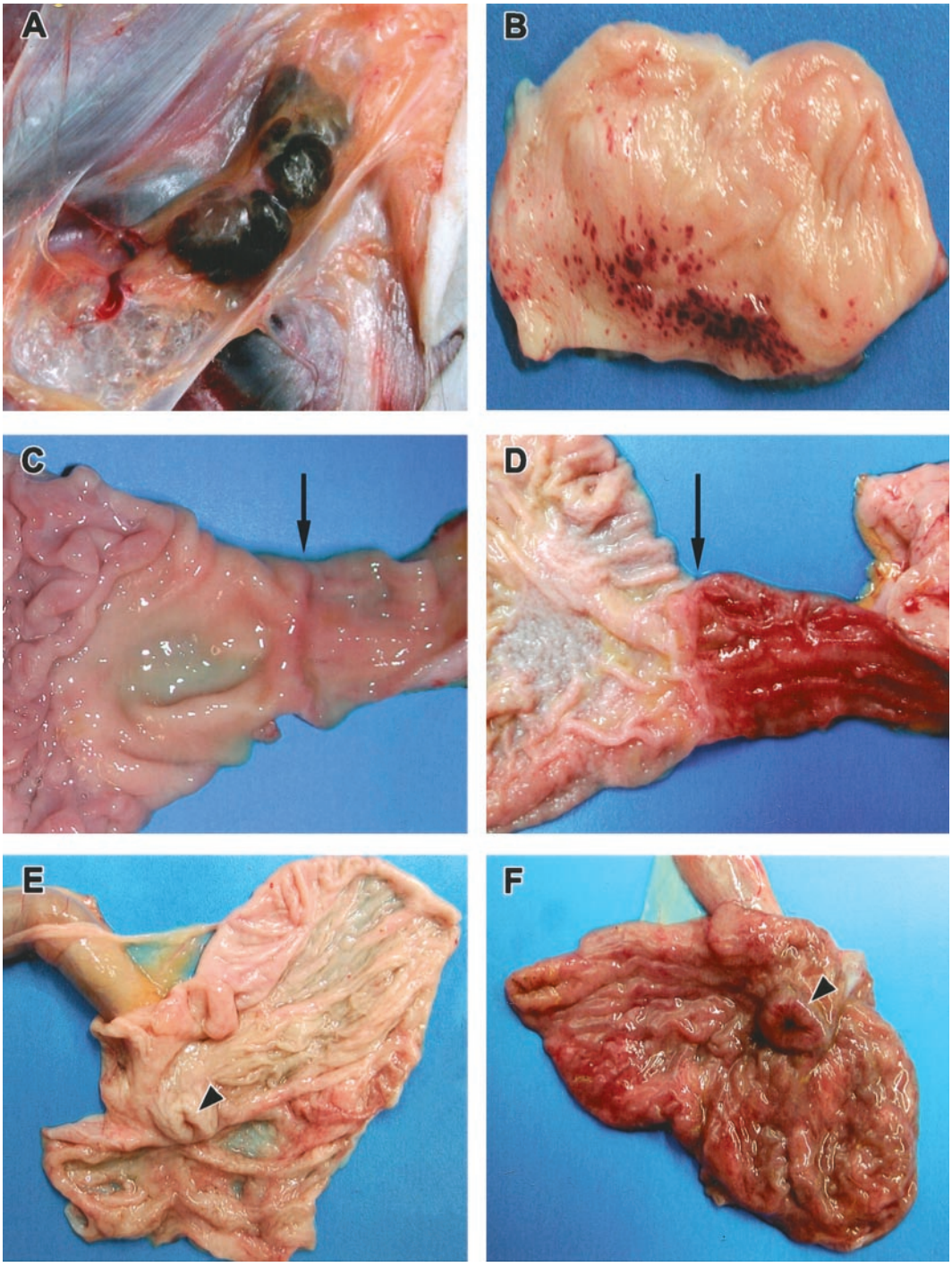

Figure 5. Representative gross necropsy lesions from cynomolgus monkeys experimentally infected with EBOV-Zaire. **A:** Mild enlargement and marked congestion/hemorrhage of inguinal lymph nodes at day 4. **B:** Multifocal to coalescing hemorrhages of mucosa of urinary bladder at day 5. **C** and **D:** Progression of marked congestion of the duodenum occurring between day 3 (**C**) and day 5 (**D**). **Arrows** indicate the gastroduodenal junction demarcating the stomach to the left and the duodenum to the right. The duodenum is markedly congested at day 5 (**D**). **E** and **F:** Progression of congestion of cecum occurring between day 3 (**E**) and day 5 (**F**). The cecum is opened up and the ileum extends outward from the cecum. **Arrowheads** indicate the ileocecal junction. Note the congested and thickened appearance of the cecum at day 5 (**F**).

2.5). Peak viremia (mean 6.9 $\log_{10}$ pfu/ml) occurred on day 6 (Figure 6). While virus was associated with peripheral blood leukocytes, this interaction was not quantitated. In tissues, infectious virus was first detected on day 2 in spleen, inguinal lymph node, and mesenteric lymph node, suggesting that these organs are early sites of viral replication; and on day 3 in axillary lymph node, mandibular lymph node, liver, lung, and bone marrow (Figure 6). Mean organ titers increased progressively and reached their highest levels (5.5–8.6 $\log_{10}$ pfu/g) on day 6. The highest titers were documented in the spleen, followed by liver, the various lymph nodes, and adrenal gland.

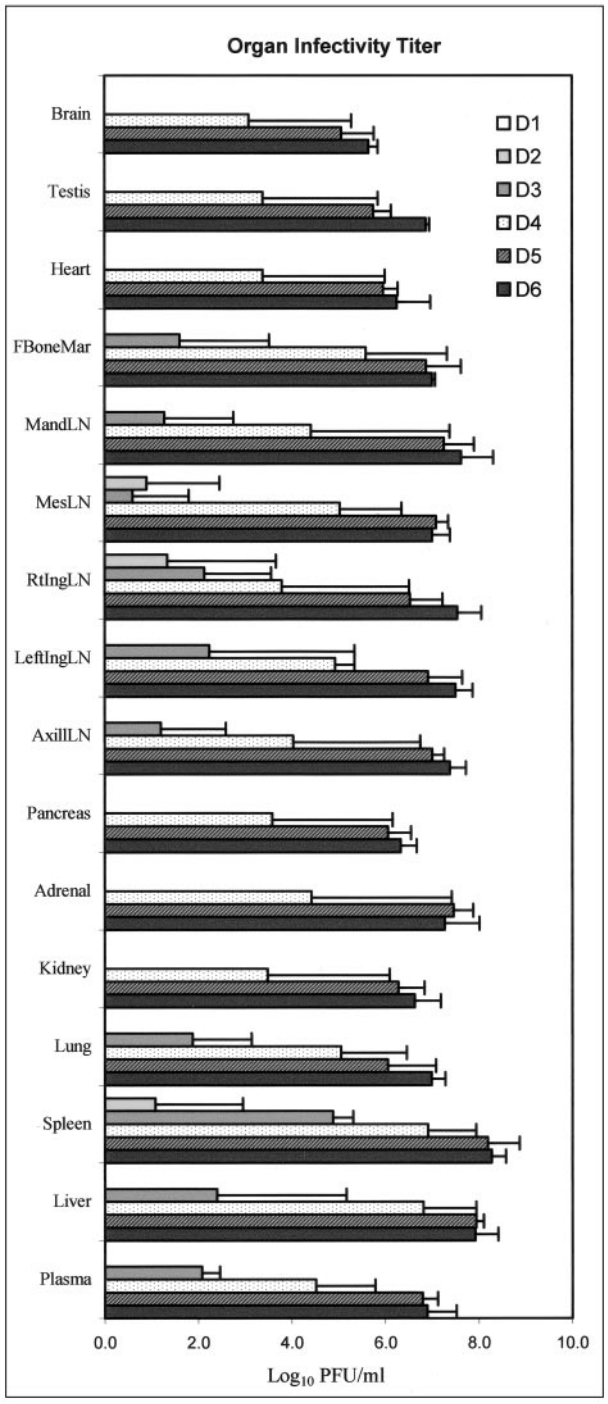

Figure 6. Mean infectivity of cynomolgus monkey plasma and tissue homogenates (10% w/v) inoculated with EBOV-Zaire. LN, lymph node.

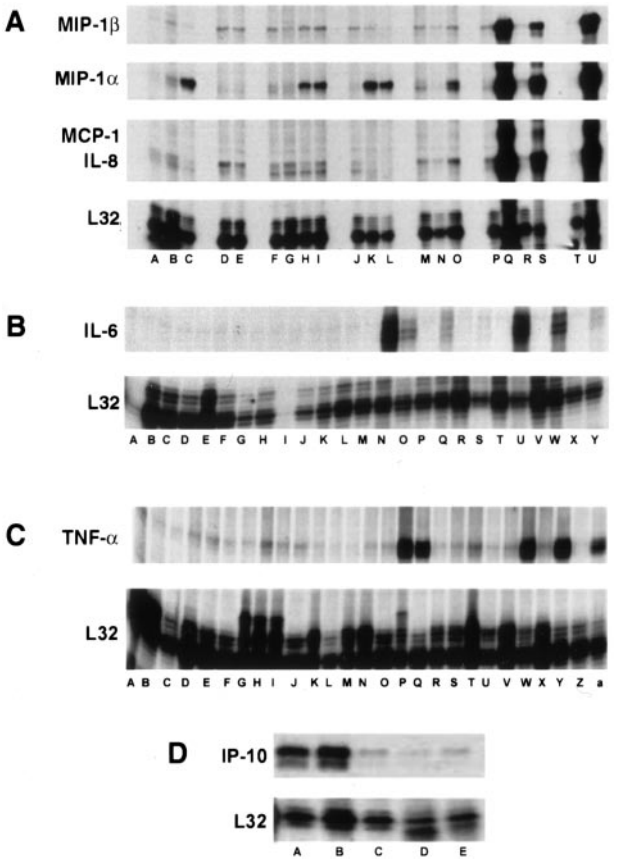

Figure 7. Analysis of mRNA of cynomolgus monkey PBMC before and after infection with EBOV-Zaire. Representative RNase protection assays are shown. **A:** Chemokines. Comparison of preinfection PBMC (**lanes A**, **D**, **F**, **J**, **M**, **P**, **T**) with PBMC at postinfection day 1 (**lanes B**, **E**, **G**); day 2 (**lanes H**, **N**, **R**); day 3 (**lanes C**, **I**, **K**, **O**); day 4 (**lanes L** and **Q**); day 5 (**lane U**); and day 6 (**lane S**). **B:** IL-6. Comparison of preinfection PBMC (**lanes A**, **D**, **F**, **I**, **L**, **P**, **R**, **T**, **V**, **X**) with PBMC at postinfection day 1 (**lanes B** and **G**); day 2 (**lanes C**, **E**, **J**, **M**); day 3 (**lanes H** and **K**); day 4 (**lanes N**, **Q**, **S**); day 5 (**lanes U** and **W**); and day 6 (**lanes O** and **Y**). **C:** TNF-α. Comparison of preinfection PBMC (**lanes A**, **C**, **F**, **H**, **K**, **N**, **R**, **T**, **V**, **X**, **Z**) with PBMC at postinfection day 1 (**lanes B**, **D**, **I**); day 2 (**lanes E**, **G**, **L**, **O**); day 3 (**lanes J** and **M**); day 4 (**lanes P**, **S**, **V**); day 5 (**lanes W** and **Y**); and day 6 (**lanes Q** and **a**). **D:** IP-10. Comparison of PBMC at postinfection day 1 (**lane A**), day 3 (**lane B**), day 4 (**lane C**), day 5 (**lane D**) and day 6 (**lane E**).

Analysis of Cytokines/Chemokines, Nitrate, and Endotoxin in Circulation

To evaluate the immune response to EBOV challenge, total RNA from extracted circulating PBMC was analyzed for an array of immunoregulatory transcripts. Plasma and/or sera were also analyzed for levels of cytokines/chemokines. Increased mRNA transcripts for MIP-1α (Figure 7A) and M-CSF were detected in some of the animals (3 of 4 and 2 of 4, respectively) by day 2, and were observed in all animals by day 3. Transcripts for IL-6 (Figure 7B), IL-8 (Figure 7A), IL-15 (not shown), MCP-1 (Figure 7A), MIP-1β (Figure 7A), and γc (not shown) were observed by day 4 in all monkeys, while increased transcripts for TNF-α were noted in some animals at day 4 (2 of 4), but were not consistently seen until days 5 and 6 (Figure 7C). Transcripts for IP-10 (Figure 7D) and RANTES were unchanged through day 3 and then appeared to decline at days 4 to 6. Transcripts for TGFβ1 increased slightly at day 2 and returned to baseline levels by day 4. Changes in levels of transcripts for IL-1α, IL-1β, IL-10, IL-13, GM-CSF, leukotriene B4, and TNF-β were not detected in any of the monkeys.

No detectable increases in plasma/sera levels of cytokines/chemokines were observed early (days 1 or 2) in the disease course. Results were recorded as positive if

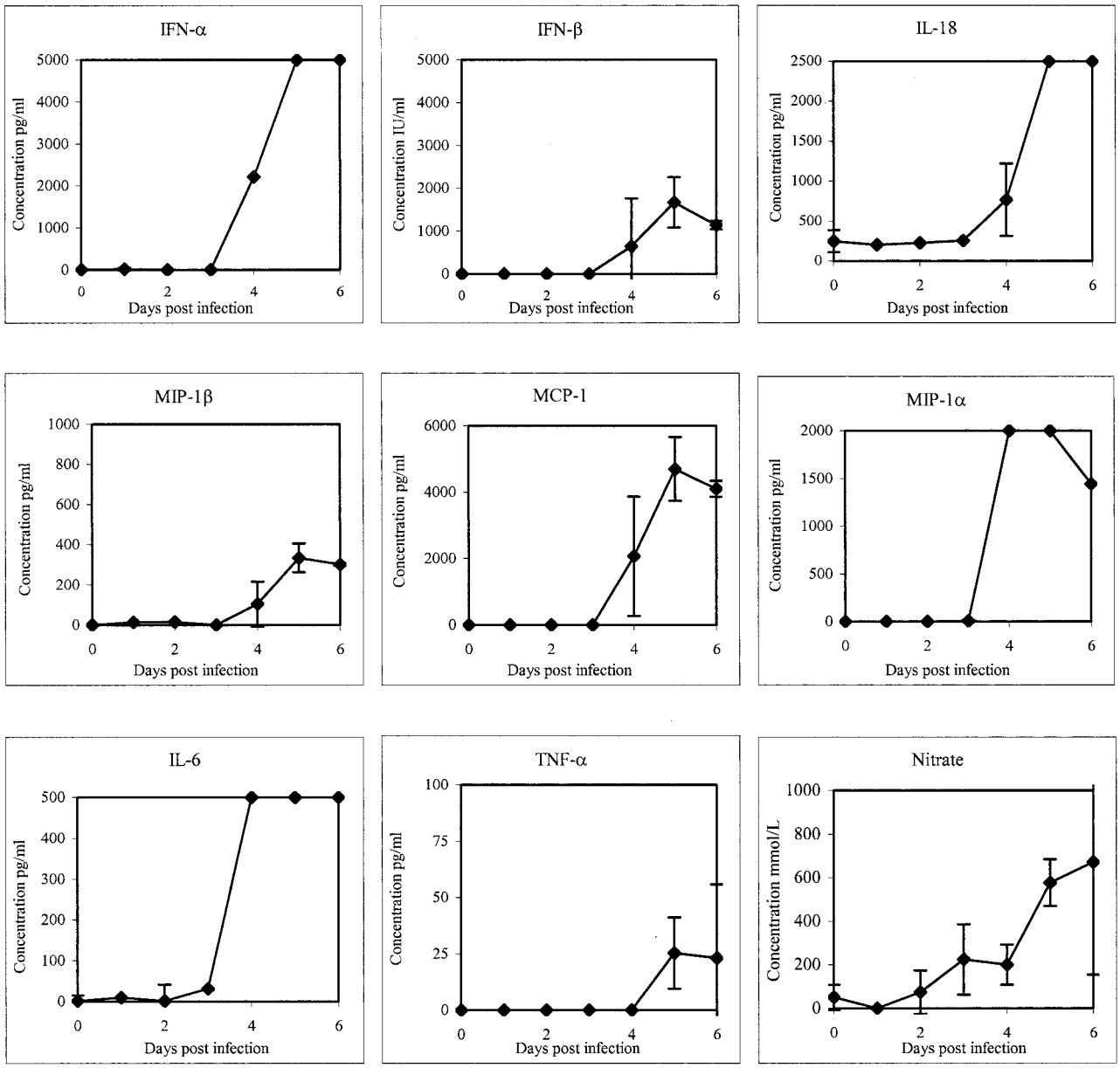

Figure 8. Analysis of cytokine/chemokine and nitrate accumulation in serum/plasma of EBOV-Zaire-infected cynomolgus monkeys.

OD values were greater than twice the OD of pre-EBOV challenge controls. At day 3, elevated levels of IL-6 were detected in 3 of 3 monkeys. At day 4, levels of IL-6 (>500 pg/ml) had markedly increased (3 of 3) and these highly elevated levels were maintained through the course of infection (Figure 8). Increased levels of IFN-α (3 of 3) (Figure 8), MIP-1α (3 of 3) (Figure 8), and IL-2 (1 of 4) were also detected at day 4. By days 5 and 6, levels of IFN-α were highly elevated (>5000 pg/ml) in sera of all monkeys; increased levels of TNF-α (>25 pg/ml) were also observed in all animals, as were levels of IFN-β (>1000 IU/ml), IL-18 (>2500 pg/ml), MCP-1 (>4000 pg/ml), and MIP-1β (> 300 pg/ml) (Figure 8). Increases in levels of IL-2 were detected in 1/3 monkeys at day 5 and 1/2 animals at day 6, while increased levels of IFN-γ were only observed at day 6 (2 of 2). Increased levels of IL-1β, IL-4, IL-8, IL-10, and IL-12 were not detected in any animal at any time point.

To assess the potential involvement of nitric oxide in EBOV pathogenesis, nitrate levels in plasma were measured as a marker for nitric oxide synthase (NOS). Analysis of the macaque samples demonstrated increased levels of nitrate (>200 mmol/L) by day 3 (3 of 3) (Figure 8). At day 5, levels of nitrate (>550 mmol/L) had further increased (3 of 3) (Figure 8). Endotoxin levels were also measured in these animals, but increased levels were not detected in serum or plasma of any monkey tested at any time point during the study.

Table 2. Histopathologic and Immunohistochemical Findings from Cynomolgus Monkeys Infected with Ebola Virus

Animal number	Days p.i.	Lymph nodes (Inguinal)			Spleen			Liver			Adrenal			Kidney		
CQ9877	1	<	0	−	<	0	−	<	0	−	<	0	−	<	0	−
CQ9890	1	<	0	−	<	0	−	<	0	−	<	0	−	<	0	−
0717CQ	1	<	0	−	<	0	−	<	0	−	<	0	−	<	0	−
CQ9846	2	3.0	0	−	2.2	0	−	<	0	−	<	0	−	<	0	−
0331CQ	2	<	0	−	<	0	−	<	0	−	<	0	−	<	0	−
CQ9028	2	<	0	−	<	0	−	<	0	−	<	0	−	<	0	−
32Q	3	1.7	0	−	4.0	0	+	3.8	0	+	<	0	−	<	0	−
CQ8667	3	2.1	0	+	4.1	0	+	3.8	0	+	<	0	−	<	0	−
CQ9093	3	<	0	−	3.3	0	+	<	0	+	<	0	−	<	0	−
CQ8681	3	5.6	0	+	4.2	0	+	<	0	+	<	0	−	<	0	−
28–427	4	3.4	0	−	4.7	1	+	4.5	1	+	<	0	−	<	0	−
CQ9887	4	5.3	3	+	6.2	3	+	6.2	2	+	5.2	1	+	3.8	1	+
CQ9108	4	4.3	3	+	5.5	3	+	5.4	2	+	4.1	1	+	2.1	1	+
CQ9095	4	4.1	2	+	7.2	3	+	7.1	3	+	5.4	0	+	5.0	1	+
28–221	5	5.3	4	+	6.5	4	+	6.9	4	+	6.2	2	+	5.1	1	+
0359CQ	5	5.4	4	+	6.8	4	+	6.7	4	+	6.1	1	+	4.6	1	+
0323CQ	5	6.9	4	+	7.4	4	+	7.1	4	+	7.0	1	+	5.9	1	+
48–143	5	6.1	4	+	8.0	4	+	7.0	4	+	6.5	2	+	5.5	1	+
CQ9878	6	6.1	4	+	7.1	5	+	6.4	4	+	6.0	2	+	5.5	1	+
28–332	6	7.1	4	+	7.6	5	+	7.0	4	+	7.1	2	+	6.3	1	+
CQ9112	6	6.5	4	+	7.1	4	+	7.3	4	+	5.7	2	+	5.0	2	+

Data are presented as tissue viral titer (log_{10} PFU/g tissue), histopathologic severity (1, minimal; 5, severe), and immunohistochemical result (+, positive; −, negative). < indicates viral titer below the detectable limit of 1.7 log_{10} PFU/g tissue.

Histology, Immunohistochemistry, in Situ *Hybridization, and Ultrastructure*

The principal histopathological and immunohistochemical findings and their association with viral isolation are presented in Table 2. Temporal results of EBOV-infected cells demonstrated in primary target tissues by immunohistochemistry and *in situ* hybridization are shown in Table 3.

Lymphoid Tissues

Lymph Nodes

By *in situ* hybridization (ISH), EBOV RNA was detected within 48 hours in a single sinus macrophage in the mesenteric lymph node of 1 of 3 monkeys. At day 3, immunohistochemistry (IHC) showed foci of immunopositive macrophages (Figure 9A and Figure 10A) and den-

Table 3. Immunohistochemical and in Situ Hybridization Findings from Cynomolgus Monkeys Infected with Ebola Virus

Animal number	Days P.I.	Lymph nodes			Spleen			Liver/adrenal		
		Mono	Mac	DC	Mono	Mac	DC	Kup	Hep	Cort
CQ9877	1	−	−	−	−	−	−	−	−	−
CQ9890	1	−	−	−	−	−	−	−	−	−
0717CQ	1	−	−	−	−	−	−	−	−	−
CQ9846	2	−	−	−	−	−*	−	−	−	−
0331CQ	2	−	−	−	−*	−	−	−	−	−
CQ9028	2	−	−*	−	−	−*	−	−*	−	−
32Q	3	−	−	−	−	++	++	++	−	−
CQ8667	3	+	+	+	++	++	++	++	−	−
CQ9093	3	−	−	−	−	++	++	++	−	−
CQ8681	3	−	−	−	−	++	++	++	−	−
28–427	4	−	−	−	−	++	++	++	−	−
CQ9887	4	+++	+++	+++	+++	+++	+++	+++	+	−
CQ9108	4	+++	+++	+++	+++	+++	+++	+++	−	−
CQ9095	4	+++	+++	+++	+++	+++	+++	+++	+	−
28–221	5	+++	+++	+++	+++	+++	+++	+++	++	++
0359CQ	5	+++	+++	+++	+++	+++	+++	+++	++	++
0323CQ	5	+++	+++	+++	+++	+++	+++	+++	++	++
48–143	5	+++	+++	+++	+++	+++	+++	+++	++	++
CQ9878	6	+++	+++	+++	+++	+++	+++	+++	++	++
28–332	6	+++	+++	+++	+++	+++	+++	+++	++	++
CQ9112	6	+++	+++	+++	+++	+++	+++	+++	++	++

+, EBOV RNA- and antigen-positive cells were rarely detected; ++, EBOV-positive cells were occasionally detected; +++, EBOV-positive cells were frequently detected; −, no EBOV-positive cells were detected.

*, EBOV RNA was detected in cells that were negative for EBOV antigen.

Mono, monocytes; Mac, macrophages; DC, dendritic cells; Kup, Kupffer cells; Hep, hepatocytes; Cort, adrenal cortical cells.

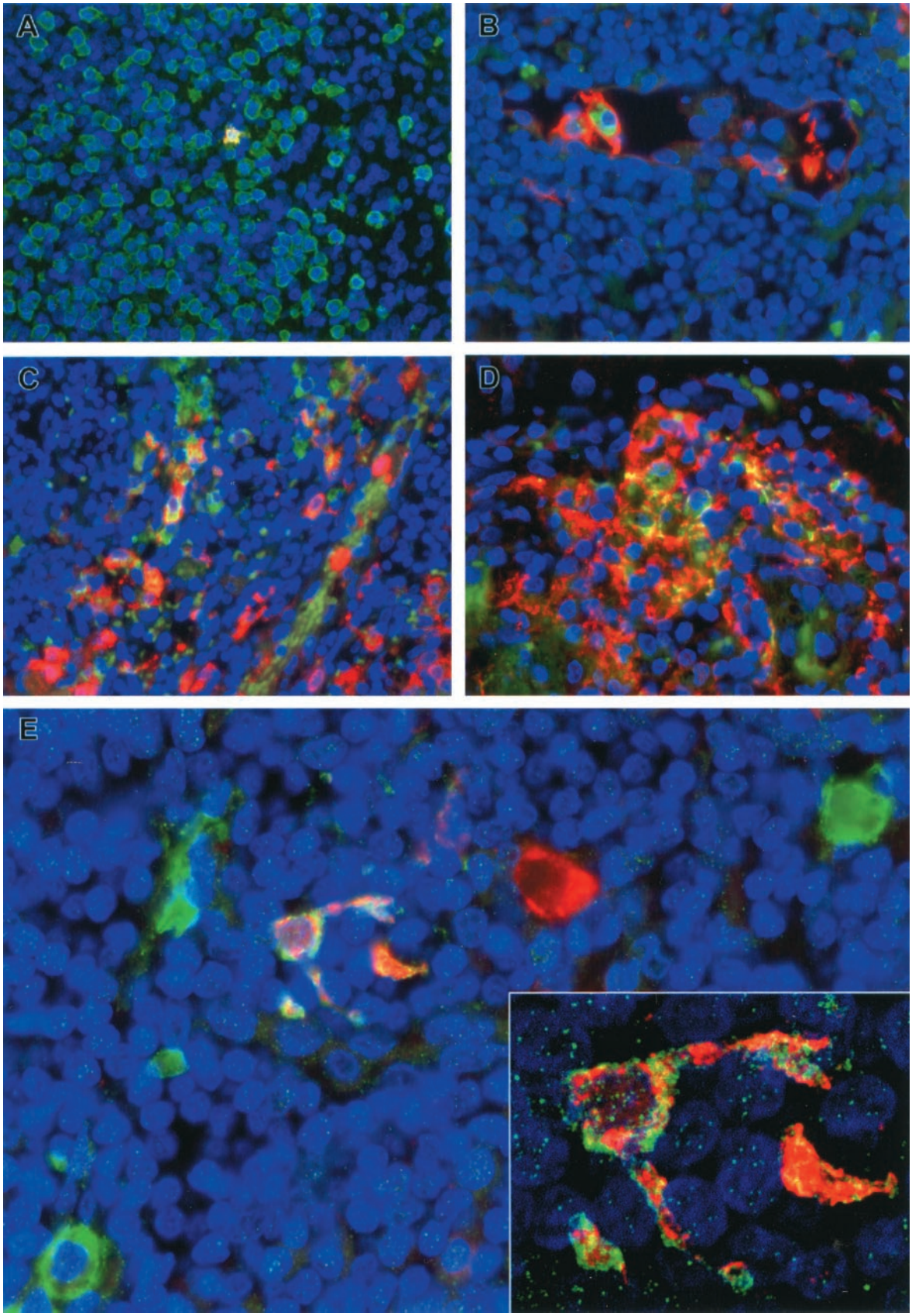
A
B
C
D
E

dritiform cells in the cortical sinuses of the left inguinal lymph node of 1 of 4 animals. Rare immunopositive macrophages and dendritiform cells were seen in cortical sinuses of the right inguinal node, and axillary and mesenteric nodes of this animal. Although no single marker thus far uniquely identifies dendritic cells (DC), a C-type lectin, DC-SIGN, is highly expressed on primate DC, and is only found on specialized macrophages in the alveoli and decidua.[31] Immunofluorescence analysis (IFA) showed that the EBOV-positive dendritiform cells in these lymph nodes were also positive for DC-SIGN (Figure 9B).

In axillary, inguinal, mandibular, mediastinal, and mesenteric lymph nodes, the first histological changes were noted at day 4. The subcapsular, cortical, and medullary sinuses contained extravasated red blood cells with evidence of erythrophagocytosis (3 of 4) and hemosiderosis (1 of 4), areas of multifocal congestion (2 of 4), and small numbers of neutrophils were present in the sinuses of the mediastinal lymph node (1 of 4), and apoptotic bodies and tingible body macrophages were multifocally present in follicles of mesenteric and inguinal lymph nodes (2 of 4). Immunoreactive macrophages were present in subcapsular, cortical, and medullary sinuses of all nodes (3 of 4) at day 4 (Figure 9C). EBOV-positive DC (Figure 9, D and E; Figure 10B) and spindle-shaped cells interpreted as fibroblastic reticular cells (FRC) were multifocally present in the paracortex (sparing the follicles) of all nodes (3/4); these immunoreactive cells were most frequently present in paravascular regions adjacent to high endothelial venules (HEV). EBOV-positive fibrocytes were noted in the mandibular lymph node capsule of one animal. ISH corroborated the IHC findings at day 4. Ultrastructurally, characteristic EBOV inclusion material[32] was detected in sinus macrophages and in cells morphologically consistent with DC.[33,34] Immunoelectron microscopy demonstrated that these EBOV-infected DC were positive for DC-SIGN.

At day 5, depletion of germinal centers was a prominent and consistent finding in all lymph nodes (4 of 4) and varying numbers of apoptotic bodies and tingible body macrophages were noted in follicles of all animals; 2 of 4 animals had apoptotic-like bodies present within HEV of the mandibular lymph nodes. The number of previously described RNA- and EBOV antigen-positive cells increased considerably between days 4 and 5. Numerous EBOV-positive DC and sinus macrophages were detected in all lymph nodes of all 4 animals. EBOV-positive endothelial cells lining HEV were observed in all lymph nodes at day 5 (4 of 4). At day 6, apoptotic-like bodies were frequently seen in all lymph nodes and were observed in sinuses as well as follicles (4 of 4), and numbers of EBOV-positive cells increased, particularly of endothelial cells lining HEV (3 of 3).

Spleen

At day 2, EBOV RNA was seen in rare macrophages in the red pulp cords of Billroth in 2 of 3 animals and in monocytes in red pulp sinusoids in the remaining animal. By day 3, multiple small foci of antigen- and RNA-positive macrophages and DC were detected in red pulp cords of Billroth and in marginal zones (4 of 4); adjacent FRC-like cells, were also antigen-positive in one animal. On day 4, there were increased numbers of neutrophils and monocytes in the red pulp sinusoids and marginal zones (4 of 4). In 2 of 4 monkeys, basophilic nuclear debris was present in the red pulp sinusoids. Multifocally, macrophages in the red pulp and marginal zone were positive for viral RNA and antigen (4 of 4); monocytes in the red pulp were occasionally EBOV-positive (4 of 4), as were red pulp and marginal zone DC (4 of 4), and spindle-shaped cells, interpreted as FRC in the red pulp, marginal zones, and very infrequently in white pulp [in the periarteriolar lymphoid sheaths (PALS)] but sparing follicles (4 of 4). By TEM, tissue macrophages in red pulp and marginal zone occasionally contained intracytoplasmic EBOV inclusions and/or budding virions (4 of 4); EBOV inclusions and/or budding virions were sporadically seen in marginal zone cells morphologically consistent with DC (3 of 4) (Figure 11A). Immunoelectron microscopy showed positive gold-sphere labeling of these EBOV-infected DC for DC-SIGN. Of note, DC-SIGN-positive DC that contained EBOV inclusions and/or budding virions were occasionally detected in marginal zone of one monkey at day 3 (Figure 11B). Two morphologically distinct populations of EBOV-infected, DC-SIGN-positive cells were seen in marginal zones at days 3 and 4. One population had typical dendritic-like processes with an electron-dense cytoplasm and few organelles (Figure 11A). The other population did not show the obvious dendritic-like processes and had a pale cytoplasm with few organelles, but were more consistently positive for DC-SIGN (Figure 11B). This population was not as easily identifiable by conventional TEM, but was evident when fields were compared in parallel with DC-SIGN-positive cells shown by immunoelectron microscopy (Figure 11C).

At day 5, there were considerable histological changes noted in the spleen of all four monkeys. White pulp was characterized by diffuse, mild to moderate, lymphoid depletion and numerous apoptotic-like bodies present in follicular center remnants. Large fibrin deposits and histiocyte necrosis/loss were prominent histological features in cords of Billroth and marginal zones (4 of 4); multifocal hemorrhage and/or congestion were also noted in marginal zones (4 of 4). Numerous apoptotic-like bodies were present in the red pulp (4 of 4) and nucleated red

Figure 9. Immunofluorescence staining of inguinal lymph nodes of EBOV-Zaire-infected cynomolgus monkeys for cell markers and EBOV. **A**: Double labeling for a macrophage marker (green) and EBOV antigens (red). Areas positive for both macrophage markers and EBOV antigens are stained gold as shown in the single EBOV-positive macrophage at day 3. **B** and **D:** Double labeling for a dendritic cell marker (DC-SIGN) (red) and EBOV antigens (green) showing a circulating EBOV-positive dendritic cell at day 3 (**B**) and large numbers of EBOV-positive dendritic cells (orange/gold) at day 5 (**D**). **C:** Double labeling for a macrophage marker (red) and EBOV antigens (green) demonstrating EBOV-positive macrophages (orange/gold) at day 5. **E:** Double labeling for a dendritic cell marker (DC-SIGN) (green) and EBOV antigens (red) demonstrating EBOV-positive dendritic cell (orange/gold) at day 4. Also, note EBOV-positive cell (red) with macrophage-like morphology and EBOV-negative dendritic cells (green) in this field. **Inset:** high-power view of the EBOV-positive dendritic cell in **E** by confocal microscopy. The nuclei were stained with DAPI (blue) in all panels. Original magnifications: ×40 (**A** and **D**); ×60 (**B**, **C**, **E**); ×300 (**inset**).

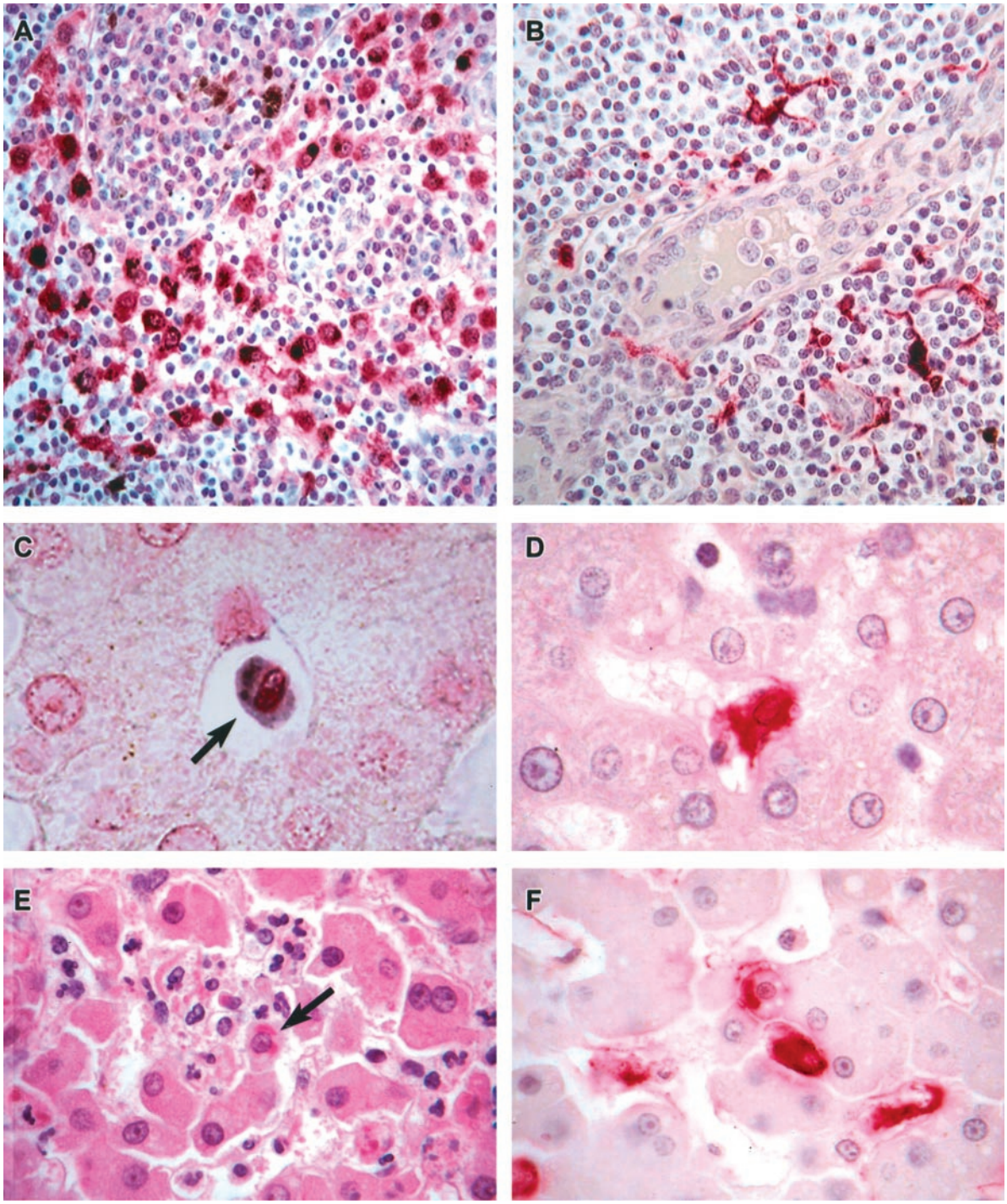

Figure 10. Localization of EBOV in cynomolgus monkey tissues. **A:** Immunopositive mononuclear cells (red) in the medullary sinus of a lymph node at day 3. The brown-pigmented cells are hemosiderin-laden macrophages. **B:** Immunopositive (red) dendritic cells surrounding a high endothelial venule in a lymph node at day 4. **C:** EBOV RNA-positive circulating monocyte (**arrow**) in hepatic sinusoid at day 2. **D:** Immunopositive (red) Kupffer cell at day 3. **E:** Histology of liver showing small foci of hepatocellular degeneration and necrosis and foci of pleomorphic eosinophilic intracytoplasmic inclusions (**arrows**) in hepatocytes at day 5. **F:** Immunopositive Kupffer cells (red) and hepatocytes (red) at day 5. Alkaline phosphatase method, **A**, **B**, **D**, **F**; H&E stain, **E**. Original magnifications: ×20 (**A**); ×40 (**B**); ×60 (**C** to **F**).

blood cells were occasionally observed in red pulp sinusoids and marginal zones (4 of 4). The number of viral RNA- and antigen-positive macrophages, DC, and FRC in the red pulp and marginal zone (4/4) were markedly increased, but continued to be infrequent in the PALS of the white pulp, between days 4 and 5; endothelial cells were very infrequently immunoreactive (4 of 4) at day 5. Ultrastructurally, EBOV inclusions were frequently seen in tissue macrophages in red pulp and marginal zone (4 of 4) and occasionally seen in marginal zone cells that were morphologically consistent with DC (4 of 4). Free virions were abundant in extracellular spaces and were often

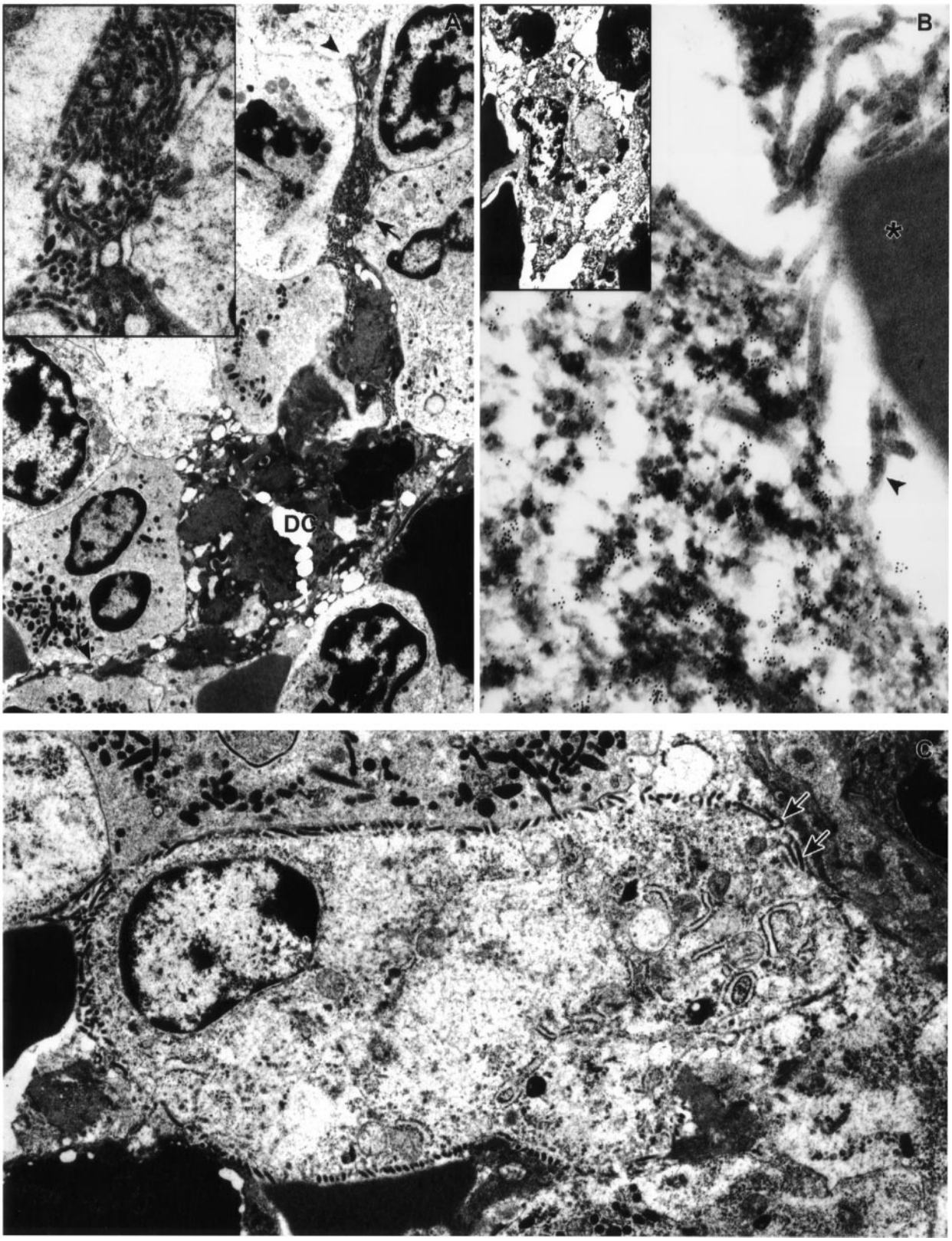

Figure 11. Ultrastructural appearance of dendritic cells in marginal zone of spleen of EBOV-Zaire-infected cynomolgus monkeys. **A:** EBOV-infected dendritic cell at day 4 with typical branching processes (**arrowheads**). **Inset**: Enlargement of area marked by **arrow** in **A** shows virions budding from plasma membrane. **B:** Immunoelectron microscopy showing positive gold sphere (10 nm) labeling of plasma membrane and cytoplasm of EBOV-infected dendritic cell for DC-SIGN at day 3. Note virions budding from plasma membrane (**arrowhead**) and near absence of gold spheres on adjacent red blood cell (*). **Inset**: Low-power view of EBOV-infected, DC-SIGN-positive pale-staining cell interpreted as an immature dendritic cell. **C:** EBOV-infected pale-staining cell interpreted as an immature dendritic cell at day 3. Morphology is comparable to DC-SIGN positive cell in **inset** of **B**. Note virions budding from plasma membrane (**arrows**), pale-staining cytoplasm, and sparsity of organelles. Original magnifications: ×6,500 (**A** and **B**, **inset**); ×12,500 (**C**); ×16,000 (**A**, **inset**); ×53,000 (**B**).

enmeshed among fibrin and fibrinocellular debris. Viral antigen and RNA persisted in macrophages and DC at day 6 as did the histological abnormalities. Additional histological changes included the appearance of lymphoblasts in periarteriolar sheaths and marginal zones (2 of 3).

Mucosal-Associated Lymphoid Tissue

No histological lesions were noted in the tonsils at day 4; however, EBOV-positive macrophages, DC, and FRC, were occasionally observed in paravascular patterns involving the interfollicular areas of the tonsil (3 of 4 animals). At day 5, apoptotic-like bodies were scattered throughout follicular centers of the tonsils; the distribution of RNA and antigen increased to include foci of EBOV-positive endothelial cells lining HEV (3 of 4), and rare foci of EBOV-positive tonsillar epithelium (1 of 4). Follicular center lymphoid depletion was prominent at day 6 (2 of 3), and increased numbers of EBOV-positive HEV endothelial cells (3 of 3) and tonsillar epithelium (2 of 3) were observed. Histological lesions, EBOV RNA, and antigen distribution patterns in the gut-associated lymphoid tissues were consistent with observations described for lymph nodes.

Thymus

Because our monkeys were adults, the thymus was involuted in all animals. At day 5 and day 6, small foci of EBOV-positive macrophage-like cells, dendritiform cells, and spindle-shaped cells were present in the medulla and at the corticomedullary junction of the thymus (3 of 4 and 3 of 3 animals, respectively); these cells were often seen in paravascular areas. EBOV antigen and RNA were infrequently present in endothelial cells of the thymus at day 5 and day 6 in 2 of 4 and 3 of 3 monkeys, respectively.

Gastrointestinal Tract

No significant lesions were seen at day 4; however, immunoreactive circulating monocytes were occasionally seen in all tissues of 3 of 4 monkeys. Small foci of antigen-positive macrophages and fibrocyte-like cells were detected in lamina propria of the stomach (1 of 4), ileum (1 of 4), ileocecal valve (3 of 4), cecum (1 of 4), and proximal colon (1 of 4). At day 5, foci of congestion were observed in the submucosa and lamina propria of the duodenum in 4 of 4 monkeys; and in the duodenum, jejunum, ileum, cecum, and colon of one monkey; mild hemorrhage was also noted in the submucosa of the cecum of this animal. EBOV-positive circulating monocytes were seen in tissue sections of all monkeys at day 5. Antigen-positive macrophages and fibrocyte-like cells, and infrequently endothelial cells, were seen in lamina propria of stomach (4 of 4), duodenum (4 of 4), jejunum (4 of 4), ileum (4 of 4), cecum (4 of 4), and proximal colon (4 of 4). Gastrointestinal tract changes at day 6 also included scattered apoptotic-like bodies in intestinal lamina propria with multifocal intraepithelial apoptotic bodies interpreted to be apoptosis of intraepithelial lymphocytes (2 of 3); occasional presence of immunopositive fibrocytes and endothelial cells in the tunica submucosa, tunica muscularis, and tunica serosa (3 of 3); and fibrin thrombi in submucosal vessels of the duodenum with associated degeneration/necrosis of Brunner's glands (1 of 3).

Liver

No significant hepatic lesions were present at days 2 or 3; however, viral RNA was detected in rare circulating monocytes at day 2 (1 of 3 animals) (Figure 10C). Viral antigen and RNA were detected in infrequent Kupffer cells of all 4 monkeys by day 3 (Figure 10D). At day 4, increased numbers of neutrophils and monocytes were seen in sinusoids and central veins (4 of 4). The number of immunoreactive Kupffer cells increased considerably between days 3 and 4 (3 of 4). Of note, small strands of fibrillar material, interpreted to be fibrin, were co-localized with these immunopositive Kupffer cells; the strands appeared to extend from the cell surface into the lumen of the sinusoid. Monocytes in the portal veins and sinusoids were occasionally immunoreactive (3 of 4), and very rare antigen-positive hepatocytes were observed. Ultrastructurally, sinusoids occasionally contained fibrin deposits, fibrinocellular debris, and free virions; the association of fibrin with EBOV-infected Kupffer cells was confirmed. Hepatocytes with intracytoplasmic filoviral inclusions were detected in rare fields of 2 of 4 monkeys.

By day 5, the histological changes also included small foci of hepatocellular degeneration and necrosis (4/4), degeneration/necrosis and hypertrophy of Kupffer cells (4/4), and multifocal pleomorphic eosinophilic intracytoplasmic inclusions in Kupffer cells and hepatocytes (4/4) (Figure 9E). EBOV antigen and RNA were detected in Kupffer cells (Figure 10F) and circulating mononuclear cells and less frequently in hepatocytes (Figure 10F); endothelial-like sinusoidal lining cells were rarely EBOV-positive. Occasional intrasinusoidal fibrin deposits were seen in all four animals. PTAH and electron microscopy confirmed the presence of intrasinusoidal fibrin and again showed that the fibrin was primarily associated with Kupffer cells. Ultrastructural examination also revealed that many degenerate and necrotic Kupffer cells and lesser hepatocytes contained viral inclusion material. Free virions were observed in association with Kupffer cell debris and in foci of hepatocellular necrosis. Sinusoids and Disse's spaces were expanded, and there was focal disruption of sinusoidal endothelium in areas where EBOV was present. Day 6 findings mirrored those described above for day 5; a slight increase in the number of EBOV-positive endothelial-like sinusoidal lining cells was noted and ultrastructurally, hepatocytes contained numerous lipid droplets.

Endocrine System

The adrenal glands were unremarkable until day 4, when increased numbers of intravascular neutrophils and

monocytes were noted in the cortex of two of four (2 of 4) monkeys. EBOV antigen and RNA were detected in circulating monocytes (3 of 4) and in macrophage and spindle-to-dendritiform cells (interpreted as stromal/stellate cells and DC, respectively) (3 of 4) adjacent to cortical cells in the zona glomerulosa, zona fasciculata, and zona reticularis. Rare EBOV-positive sinusoidal lining cells were seen in the cortex of 2 of 4 monkeys. In addition, EBOV RNA was detected in adrenal cortical cells in the zona fasciculata (2 of 4) and zona reticularis (1 of 4), stromal cells in the cortex (2 of 4), and fibrocytes in the capsule (1 of 4). Histopathology at day 5 included mild, multifocal congestion of the adrenal cortex (4 of 4) and multifocal degeneration and necrosis of adrenal cortical cells with rare eosinophilic intracytoplasmic inclusions and acute inflammation (2 of 4). In addition to the nonendocrine cells described above, individual and small foci of antigen-positive adrenal cortical cells were present in the zona glomerulosa, zona fasciculata, and zona reticularis of the cortex at day 5 (4 of 4); in multiple foci, a thin line of immunoreactivity appeared to separate cortical cells (4 of 4); this staining was interpreted to represent free intercellular virions, and was subsequently confirmed by electron microscopy. Day 6 histopathology and antigen distribution were similar to day 5 (3 of 3). EBOV was not detected in pituitary gland, thyroid gland, or pancreatic islets of any animal by either IHC or ISH.

Kidneys and Urinary Bladder

The kidneys were unremarkable until day 4 when mild, multifocal congestion was noted in three of four (3 of 4) monkeys and fibrin thrombi, confirmed by PTAH staining, were infrequently present in medullary vessels (2 of 4). Circulating monocytes contained EBOV antigen and RNA (3/4). Multifocally, proximal convoluted tubular epithelial cells were antigen-positive but viral RNA-negative (2/4); previous studies have shown that this staining is likely a result of secretion or reabsorption of VP40 by tubular epithelium and not due to viral infection of these cells.[35] The urinary bladder was histologically normal at day 4; however, immunopositive circulating monocytes were detected in 3 of 4 monkeys. At day 5, fibrin thrombi, confirmed by PTAH staining, were multifocally present in renal medullary vessels (3 of 4). Viral antigen was detected in rare endothelial cells of the capillaries of the renal medulla (1 of 4), and as described above, viral antigen but not viral RNA, was observed in proximal convoluted tubular epithelial cells (4 of 4). Small hemorrhages were noted in the urinary bladder lamina propria of 1 of 4 monkeys at day 5. RNA- and antigen-positive macrophages (1 of 4) in the urinary bladder lamina propria and infrequent positive fibrocytes (3 of 4) and endothelial cells (1 of 4) in the lamina propria, tunica mucosa, and tunica serosa were present at day 5. By day 6, EBOV RNA and antigen were present in fibrocytes and macrophage-like cells in the interstitium of the renal cortex and medulla and in the connective tissue of the renal pelvis (3 of 3). Endothelial cells lining capillaries in the medulla and cortex were infrequently EBOV-positive in 3 of 3 monkeys; 1 of 3 animals showed small hemorrhages in the lamina propria of urinary bladder. The distribution of viral RNA and antigen intensified in the urinary bladder at day 6 in 2 of 3 animals. Multiple foci of EBOV-positive macrophages, fibrocytes, and endothelial cells were observed in the connective tissue of the lamina propria, tunica muscularis, and tunica serosa.

Other tissues

Bone marrow was unremarkable until day 4 when a decreased ratio of nonproliferating maturation storage pool to proliferating pool was observed in the myeloid series cells (3 of 4 animals). This histological finding, interpreted as a depletion of the storage pool, was consistent in all monkeys at days 5 and 6. Multifocally, bone marrow macrophages and stromal cells contained EBOV antigen and RNA in 3 of 4 monkeys at day 4 and in all animals at days 5 and 6.

No significant pathology was seen in the respiratory system, the reproductive system, the central and peripheral nervous system, skin and adnexa, tongue and esophagus, or heart. Immunohistochemistry and *in situ* hybridization findings were similarly unremarkable in these tissues. By days 5 and 6, individual and small foci of EBOV RNA- and antigen-positive macrophages, DC, and fibroblast-like cells were detected in most of these tissues in all animals examined (4 of 4 at day 5, and 3 of 3 at day 6). EBOV-positive germinal epithelial cells were infrequently noted in tongue of 1 of 4 animals at day 5, and tongue, esophagus, and lip of 1 of 3 animals at day 6.

Evaluation of Apoptosis

Blood

PBMC were evaluated for evidence of apoptosis by TEM and RNA analysis. Evidence of increased apoptosis was not detected in the PBMC by TEM of any of the day 1 or 2 monkeys compared to the pre-challenge PBMC of the 21 animals. By day 3, TEM evidence of morphological apoptosis[36,37] in lymphocytes was observed in nearly every field surveyed (4 of 4). It appeared that the highest proportion of these apoptotic lymphocytes represented the large granular lymphocyte fraction and, furthermore, had ultrastructural characteristics of NK cells[38,39] (Figure 12A). Specifically, these cells were larger in cross-section (6 to 8 μm) and had abundant cytoplasm that contained granules not seen in other lymphoid cells, and an abundance of mitochondria and polyribosomes. TEM of day 4 PBMC showed increased numbers of apoptotic small lymphocytes (4 to 6 μm in cross-section) and markedly elevated numbers of neutrophils (Figure 12B), which is consistent with the differential white blood cell counts. By days 5 and 6, increased numbers of apoptotic bodies were present in all fields surveyed, and many of these bodies appeared to be phagocytosed by monocytes/macrophages and neutrophils.

RNA analysis of PBMC showed several gene expression changes in apoptosis-associated signaling mole-

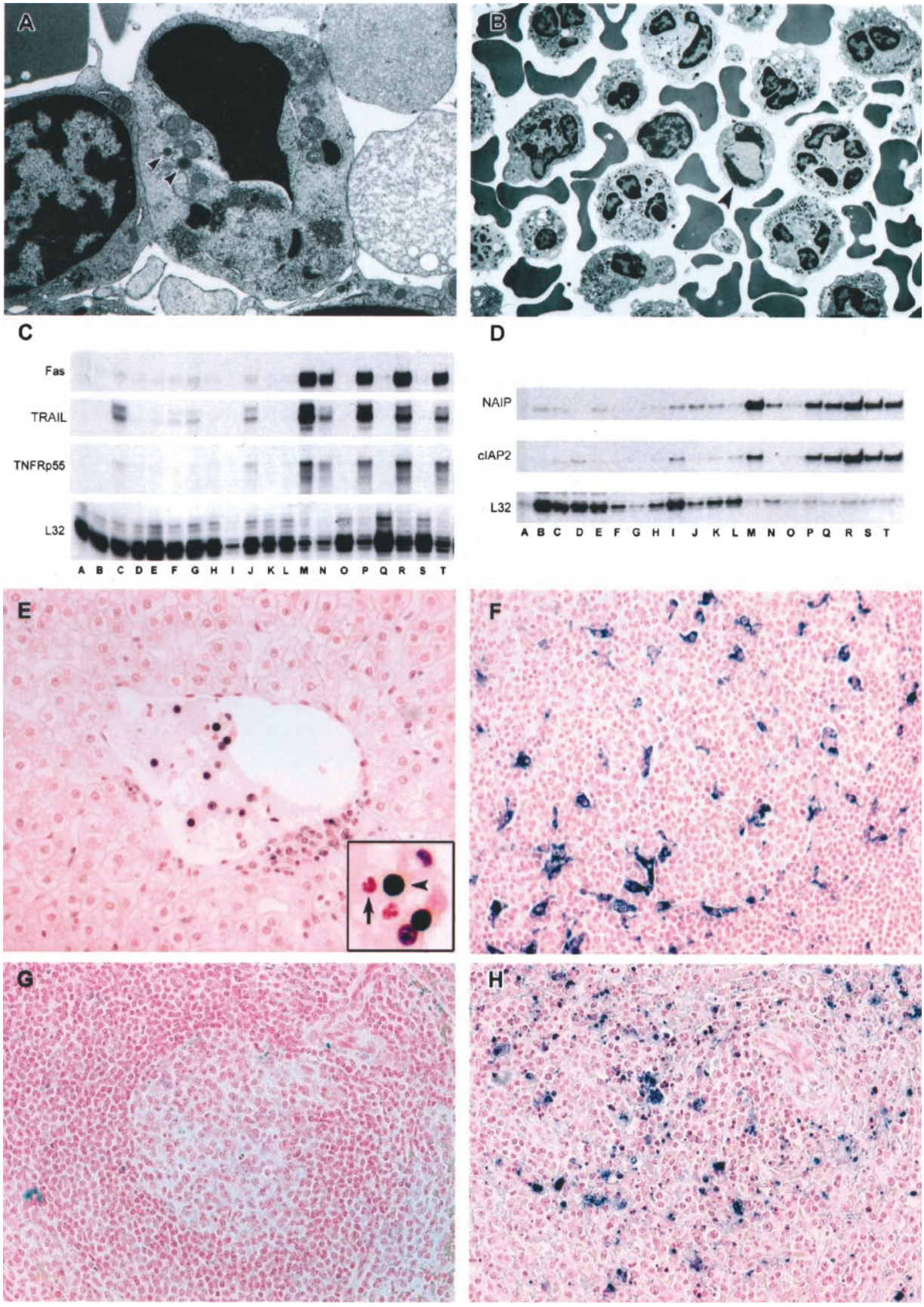
A
B
C
Fas
TRAIL
TNFRp55
L32
A B C D E F G H I J K L M N O P Q R S T
D
NAIP
cIAP2
L32
A B C D E F G H I J K L M N O P Q R S T
E
F
G
H

cules. Increased mRNA levels of the pro-apoptotic genes TNF-related apoptosis-inducing ligand (TRAIL) (Figure 12C), Fas/CD95 (Figure 12C), and receptor interacting protein (RIP) were observed by day 3 postinfection; Fas-associated death domain protein (FADD), Requiem, and Bcl-2 family proteins bik and bak were noted at later stages of disease. Transcripts for anti-apoptotic genes, cellular inhibitor of apoptosis protein 2 (cIAP-2) and neuronal apoptosis inhibitory protein (NAIP) were increased by days 2 and 3 (Figure 12D), while transcripts of Bcl-2 family proteins bfl-1, bcl-2, and mcl-1 were increased by day 4.

Tissues

No significant findings were observed at 24 hours. At day 2, there was TUNEL-labeling of apoptotic bodies in scattered Kupffer cells and infrequently in circulating monocytes in the liver of 1 of 3 monkeys. This same animal also had infrequent TUNEL-positive apoptotic bodies in splenic macrophages and DC in the follicles and paracortex of the axillary lymph node; rare TUNEL-positive lymphocytes were seen in spleen, and in follicles and sinuses of the axillary lymph node. By day 3, TUNEL-positive apoptotic bodies were multifocally detected in Kupffer cells and circulating monocytes in liver and spleen, tissue macrophages in splenic red pulp (3 of 4), DC, and macrophages in splenic white pulp (3 of 4), and macrophages in sinus and paracortex of peripheral lymph nodes (3 of 4). TUNEL-positive circulating lymphocytes were seen in multiple foci of liver (Figure 12E) and spleen, and infrequently noted in follicular centers as would be expected of peripheral lymph nodes. Ultrastructurally, macrophages containing apoptotic bodies were infrequently detected in red pulp of spleen (3 of 4) and in sinuses of inguinal lymph nodes (2 of 4); apoptotic lymphocytes were infrequently seen in sinuses of inguinal lymph nodes (2 of 4) and occasionally observed within the HEV of inguinal node of 1 of 4 animals.

By day 4, Kupffer cells and tissue macrophages in red pulp of spleen with TUNEL-positive tingible bodies were numerous in all 4 monkeys. TUNEL-positive apoptotic bodies were multifocally detected in circulating monocytes in liver and spleen (4 of 4), DC and macrophages in splenic white pulp (3 of 4), macrophages in sinuses and paracortex of peripheral lymph nodes (4 of 4), and macrophages and DC in follicular centers of peripheral lymph nodes (4 of 4) (Figure 12, F to H). TUNEL-positive circulating lymphocytes were seen in multiple foci of liver and spleen, and peripheral lymph node sinuses (4 of 4), and less frequently noted in follicular centers of peripheral lymph nodes (4 of 4). TEM confirmed TUNEL findings and also showed infrequent apoptotic plasma cells in spleen of 2 of 4 animals. TUNEL findings were similar at days 5 and 6; increased numbers of apoptotic lymphocytes, and macrophages and DC with TUNEL-positive apoptotic bodies were detected in all monkeys. The most notable difference by TEM was the abundance of apoptotic lymphocytes, which were readily detected in lymph node sinuses and paracortex.

Discussion

Histological lesions, IHC, and ISH demonstrated a similar pattern of EBOV infection, starting with monocytes/macrophages and DC in the lymphoid tissues and Kupffer cells in liver, progressing to infection of parenchymal cells in liver and adrenal gland, endothelial cells lining sinusoids in liver and adrenal gland, as well as HEV in lymphoid tissues, fibrocytes, and endothelial cells of connective tissue, and finally to infection of the epithelium. The role of endothelial cells in EBOV pathogenesis is detailed in a companion paper.[40] The current study demonstrates, for the first time, that DC are early and sustained cellular targets of EBOV in nonhuman primates; that lymphocyte apoptosis is a relatively early event in disease progression, and furthermore, it is the NK cell fraction that is likely lost through increased apoptosis early in the course of infection. Previous studies of moribund monkeys demonstrated that EBOV has a predilection for monocytes/macrophages,[6,14,41] and these cells were shown to be early and sustained targets of EBOV in guinea pigs.[11] We also observed early and sustained infection of monocytes/macrophages in the present study, with EBOV RNA initially detected in lymphoid monocytes/macrophages at day 2 postinfection. Because monocytes/macrophages are usually the cells that elicit the response cascade in the acute phase of inflammation,[42] their early infection represents an effective strategy for evasion of the host defense system as well as facilitating dissemination of the virus.

While the importance of monocytes/macrophages in EBOV pathogenesis have been well-documented,[28,30,41,43–44] few studies have addressed the importance of DC in EBOV pathogenesis; these cells also play

Figure 12. Analysis of PBMC from EBOV-Zaire-infected cynomolgus monkeys for evidence of apoptosis. **A** and **B:** Transmission electron micrographs of peripheral blood mononuclear cells. **A:** Apoptosis of a large lymphocyte (~6 × 8 μm in cross-section) morphologically consistent with a NK cell at day 3. **Arrowheads** indicate cytoplasmic granules. Also, note abundance of mitochondria. **B:** Apoptotic small lymphocyte (**arrow**) and increased numbers of neutrophils at day 4. **C** and **D:** Analysis of PBMC mRNA; representative RNase protection assays are shown. **C:** Fas and TRAIL, Comparison of preinfection PBMC (**lanes A**, **D**, **H**, **K**, **O**, **Q**, **S**) with PBMC at postinfection day 1 (**lanes B** and **E**); day 2 (**lanes F**, **I**, **L**); day 3 (**lanes C**, **G**, **J**); day 4 (**lane M**); day 5 (**lanes P** and **R**); and day 6 (**lanes N** and **T**). **D:** NAIP and cIAP2. Comparison of preinfection PBMC (**lanes A** to **C**) with PBMC at postinfection day 1 (**lanes D** to **F**); day 2 (**lanes G** to **I**); day 3 (**lanes J** to **L**); day 4 (**lanes M** to **O**); day 5 (**lanes P** to **R**); and day 6 (**lanes S** and **T**). **E** to **H:** Analyses of tissues by TUNEL assay. **E:** Apoptotic mononuclear cells (black reaction product) within the lumen of a central hepatic vein and to the periphery of the vein at day 3. **Arrow** in the **inset** points to an unaffected neutrophil and the **arrowhead** indicates the apoptotic lymphocyte. At day 4, follicles in a lymph node contain macrophages and dendritiform cells that have engulfed tingible bodies (**F**). **G:** A follicular area in spleen of an uninfected control monkey, showing little evidence of apoptosis, compared to a similar area in spleen of an EBOV-infected monkey at day 5, showing macrophages that have engulfed tingle bodies; single-strand breaks appear blue/black in **F** to **H**. Original magnifications: ×20 (**E** to **H**); ×6,500 (**B**); ×16,000 (**A**).

important roles in initiation and regulation of the host immune response. DC are a family of professional antigen-presenting cells, derived from bone marrow, which have the ability to initiate and modulate cell-mediated immune responses.[45,46] Immature DC function as sentinels of the adaptive immune system; they are located in the peripheral tissues where they capture and process exogenous antigens and migrate to regional lymph nodes where they undergo maturation. A wide variety of stimuli, including infectious virus, bacterial antigens, or inflammatory cytokines, can trigger maturation of DC, which is characterized by phenotypic changes, including up-regulation of MHC and costimulatory molecules, and production of IL-12. Presentation of acquired antigen by mature DC leads to T-cell activation.[47,48] Monocytes circulating in the blood could be equally important in the DC response as circulating monocytes counter infection by crossing the endothelial barrier, infiltrating the focus of infection, and developing either into macrophages or DC.

Regarding the importance of EBOV predilection for DC in disease pathogenesis, we speculate that EBOV acts in a manner similar to other viruses that are known to disable the host immune response by attacking and manipulating the very cells that play the most critical roles in initiating the antiviral immune response. DC-tropic viruses such as HIV,[49,50] measles virus,[51–53] LCMV,[54] Dengue,[55] cytomegalovirus,[56] and HSV1[57] have evolved mechanisms to impair the function of DC, thereby enhancing their chance to escape immune surveillance. Raftery et al[56] proposed that infection of DC by human cytomegalovirus induces immunosuppression through a multilayered defense strategy that includes partially down-regulating MHC molecules, up-regulating apoptosis-inducing ligands CD95L and TNF-related apoptosis-inducing ligand (TRAIL) to delete activated T lymphocytes, complemented by a nondeletional mechanism involving undefined viral proteins that suppresses surviving T lymphocytes. Of note, increased TRAIL expression and partial suppression of MHC II were associated with EBOV infection of immature DC *in vitro*[30]; apoptosis of bystander lymphocytes is a characteristic feature of EBOV infections[28] and furthermore, the well-chronicled discovery of an immunosuppressive motif in the C-terminal region of filoviral glycoproteins[58–60] lends some additional credence to this comparison. Thus, it is evident that the result of interactions between viruses and DC is critical for the outcomes of EBOV infections.

Profound lymphopenia and lymphoid depletion are characteristic features of EBOV HF. Extensive lymphocyte apoptosis appears to be critical to the pathogenesis of EBOV in humans and nonhuman primates.[28,61] In fatalities, widespread lymphocyte apoptosis occurs before the development of an adequate adaptive (B- and T-lymphocyte-mediated) immune response. In survivors, the adaptive immune response, arising in the absence of such pathological lymphocyte apoptosis, controls viral replication and leads to disease resolution. Of note, fatalities have markedly increased serum levels of nuclear mitotic apparatus protein (NuMA), a protein that is efficiently cleaved by caspases during classical and granzyme B-mediated caspase-independent apoptosis.[62,63] In this study, as in a previous study,[28] we have clearly shown that massive lymphocyte apoptosis is recapitulated in macaques experimentally infected with EBOV. In rhesus and cynomolgus monkeys, there is lymphopenia and lymphocyte depletion/loss in lymphoid tissues. Apoptosis is evident in lymphocytes, both in the vasculature as well as in lymphoid tissue. Both classical morphology and evidence of DNA fragmentation are seen. The mechanism(s) underlying such apoptosis have been unclear. It is not due to direct viral infection; lymphocytes are not productively infected, and infected mononuclear phagocyte system cells are not apoptotic. In the current study, we found evidence of abnormal lymphocyte apoptosis in PBMC, in the vasculature, and in lymphoid tissues as early as day 3 postinfection. By days 4 to 6, a consistent increase in bystander lymphocyte apoptosis was noted in all animals.

We previously showed increased TRAIL expression in EBOV-infected adherent human monocytes/macrophages *in vitro*, and suggested that TRAIL is involved in apoptosis of host lymphocytes.[30] Analysis of apoptotic genes in this study showed increased TRAIL transcripts by day 3 postinfection in peripheral blood mononuclear cells. Type I IFNs are known to enhance TRAIL expression on human lymphocytes, making them susceptible to TRAIL-induced apoptosis,[64] and we demonstrated highly elevated plasma levels of type I IFNs in this study. Measles virus was found to induce type I IFN expression in monocytes,[65] and IFN-α treatment induced functional TRAIL expression in monocytes[66] and DC.[67] Functional TRAIL is produced by measles virus-infected DC and mediates their cytotoxic activity.[67] Killer activity is also induced by HIV infection. In fact, HIV infection of human DC leads to release of an as yet unidentified soluble factor(s), which induces apoptosis of thymocytes and activated peripheral blood mononuclear cells.[68] TRAIL involvement in this killer activity has not been tested yet, but increased sensitivity of T cells from HIV patients to TRAIL-induced apoptosis has been described.[69,70] Cytotoxic activity of either measles virus- or HIV-infected DC results in lymphocyte apoptosis and may be TRAIL mediated. Other studies have reported that IFN-α production up-regulates TRAIL production and down-regulates TRAIL receptor 2 expression[65] thus protecting monocytes from apoptosis. Furthermore, up-regulation of NAIP and cIAP2 mRNA in macaque PBMC of the current study, and in EBOV-infected primary human monocytes/macrophages *in vitro* (T. W. Geisbert, unpublished observation), suggests that EBOV has evolved an additional mechanism to resist host defenses by inducing these protective transcripts in cells that it infects. In fact, regulation of apoptosis may be part of the pathogenesis of EBOV. Current studies are ongoing to evaluate the role of these genes in promoting/resisting apoptosis of specific lymphocyte populations.

Evidence of apoptosis was not seen in any EBOV-infected DC. This finding is consistent with previous studies showing that dsRNA infection of DC exerts anti-cytopathic effects.[71,72] For example, Cella et al[72] demonstrated that DC activation by viruses such as influenza

results in the induction of type I IFN, which triggers a cellular resistance to cytopathic effects via up-regulation of MxA protein. This increased resistance allows infected DC to present corresponding antigens and to induce protective immune responses. Similarly, TNF-α can protect DC from cell death by up-regulating anti-apoptotic factors such as Bcl-xl.[73,74] Furthermore, the virus-induced production of TNF-α and IFN-α is thought to contribute to the lesser cell death in Dengue virus-infected DC in the late phase of virus infection.[55]

There is recent evidence that increased levels of nitric oxide (NO) at inflammatory sites may affect the biological activity of lymphoid cells. Specifically, recent studies showed that dissipation of mitochondrial membrane potential is an early event in apoptotic cell death, and that a high concentration of NO depressed the mitochondrial membrane potential in human peripheral blood lymphocytes inducing apoptosis.[75] Moreover, Takabayashi et al[75] showed that apoptosis and the production of reactive oxygen species was highest in NK cells. As we were able to demonstrate elevated plasma levels of nitrate (as marker for NO synthetase) in our EBOV-infected monkeys, we speculate that high concentrations of NO may trigger the bystander apoptosis and loss of NK cells as seen in the animals in this study. In addition, peroxynitrite alone, or with NO, can mediate direct toxicity as well as activated inflammatory cascades via NFκB. Combined, these events may lead to organ injury and contribute to the multiple organ failure that is characteristic of EBOV infections.

Primate EBOV infections are characterized by a dysregulation of normal host immune responses. In this study, we have shown increased circulating levels of IFN-α, IL-6, MCP-1, MIP-1α, and MIP-1β at the early- to mid-stages of disease, and IFN-β, IL-18, and TNF-α at later stages of disease. We failed to detect increased levels of IFN-γ, IL-4, IL-8, IL-10, or IL-12. Increased levels of IL-10 have been associated with fatality in previous EBOV outbreaks.[61,76] One of these studies associated increased levels of IFN-α with fatalities,[76] while the other study did not detect IFN-α, IL-1β, IL-8, or IL-12.[61] Moderate levels of IL-6 and TNF-α were associated with fatal infection in the days before death in the Gabon study,[61] and high levels of TNF-α, but not IL-6, were associated with fatality in the Kikwit investigation.[76] Increased levels of IL-2 were noted in 2 of 7 fatal cases in the Kikwit study; we noted slightly increased levels of IL-2 in 2 of 5 late-stage (days 5 and 6) monkeys. Our results are as comparable to those of these previous human studies as each of the human studies is to each other. There are some notable differences, particularly with regard to increased levels of IL-10, which were associated with fatal cases of EBOV in both human studies, while changes in IL-10 were not detected in any of our EBOV-infected cynomolgus monkeys.

Notwithstanding issues of unknown routes and doses of exposure, and pre-existing medical conditions, there are other concerns when comparing information obtained from patients during EBOV outbreaks with information gathered from nonhuman primates under experimental conditions. Clinical identification of EBOV infection, particularly in tropical settings, is problematic as initial symptoms are nonspecific and similar to those of more common infections including malaria, salmonellosis, typhoid fever, and shigellosis. A typical course of action in these cases is intervention with broad-spectrum antibiotics. However, the use of antibiotics, while clearly warranted, may confound interpretation of the immunological response to EBOV, thus, making it difficult to fully evaluate human immunopathogenesis and compare it with what is known about nonhuman primate models, where animals are not usually treated with antibiotics or given any supportive care. It is known that antibacterial agents can modify acute-phase inflammatory responses through their effects on cytokine synthesis by monocytes.[77–80] It has also been shown that antibiotic-induced changes in the gut microflora can modulate the gut cytokine production after tissue injury with or without hemorrhagic shock.[81,82]

In summary, the paradigm that we propose for EBOV pathogenesis in primates, based on results of the current study, is as follows: EBOV spreads from the initial infection site via monocytes and DC to regional lymph nodes, likely via lymphatics, and to liver and spleen via blood. At these sites, EBOV infects tissue macrophages (including Kupffer cells), DC, and FRC. EBOV activates DC early in the course of infection by up-regulating expression of TRAIL. Such overexpression of TRAIL, which is sustained as the disease progresses by overexpression of IFN-α, participates in T lymphocyte deletion via bystander apoptosis, and establishment of virus-induced immunosuppression. Concomitantly, EBOV-infected monocytes/macrophages release a variety of soluble factors, including proinflammatory cytokines such as MIP-1α and MCP-1, which recruit additional macrophages to areas of infection, making more target cells available for viral exploitation and further amplifying an already dysregulated host response. As disease progresses, increased levels of oxygen free radicals (eg, NO), released by EBOV-infected macrophages at inflammatory sites, trigger apoptosis of NK cells, thwarting the innate immune response and leaving the host little time to mount an adaptive response. Left unchecked, extensive viral replication leads to increased levels of additional proinflammatory cytokines, notably IL-6, which then trigger the coagulation cascade. Activation of the coagulation cascade, in turn, activates the fibrinogenic and fibrinolytic pathways leading to DIC. Inhibitors of the clotting system are consumed at a rate that exceeds synthesis by liver parenchymal cells, which by this point have been rendered dysfunctional by the viral assault. Left unchecked, the fibrinogenic and/or fibrinolytic coagulopathy could result in rapid progression of fibrin thrombi, and/or hemorrhagic shock, multiple organ failure, and finally, death of the host.

This sequence of morphological, cytologic, virologic, serological, and inflammatory change following EBOV infection creates a useful model in the study of experimentally induced EBOV HF and the sequence of pathogenetic events identified should provide new targets for rational prophylactic and chemotherapeutic interventions. Because of massive synergism and redundancy in

the pathways of apoptosis, inflammation, and the development of hemorrhagic shock, it is likely that combined or appropriate sequential targeting of the above-listed pathways for treatment modalities will be more effective than targeting a single pathway.

Acknowledgments

Opinions, interpretations, conclusions, and recommendations are those of the authors and are not necessarily endorsed by the U.S. Army. Research was conducted in compliance with the Animal Welfare Act and other Federal statutes and regulations relating to animals and experiments involving animals and adheres to principles stated in the Guide for the Care and Use of Laboratory Animals, National Research Council, 1996. The facility where this research was conducted is fully accredited by the Association for Assessment and Accreditation of Laboratory Animal Care International.

We thank Denise Braun, Lynda Miller, Roswita Moxley, Jeff Brubaker, Steve Moon, Neil Davis, and Larry Ostby for their expert technical assistance. We also thank Gabriela Dveksler, Aileen Marty, Rahda Maheshwari, and Chou-Zen Giam for helpful discussions and comments, and Gordon Ruthel for skillful assistance with confocal microscopy.

References

1. Bowen ETW, Lloyd G, Harris WJ, Platt GS, Baskerville A, Vella EE: Viral haemorrhagic fever in southern Sudan and northern Zaire. Lancet 1977, 1:571–573
2. Johnson KM, Lange JV, Webb PA, Murphy FA: Isolation and partial characterization of a new virus causing acute haemorrhagic fever in Zaire. Lancet 1977, 1:569–571
3. Khan AS, Tshioko K, Heymann DL, Le Guenno B, Nabreth P, Kerstiens B, Fleerackers Y, Kilmarx PH, Rodier GR, Nkuku O, Rollin PE, Sanchez A, Zaki SR, Swanepoel R, Tomori O, Nichol ST, Peters CJ, Muyembe-Tamfum JJ, Ksiazek TG: The reemergence of Ebola hemorrhagic fever, Democratic Republic of the Congo, 1995. J Infect Dis 1999, 179(Suppl 1):S76–S86
4. Bowen ETW, Platt GS, Simpson DIH, McArdell LB, Raymond RT: Ebola haemorrhagic fever: experimental infection of monkeys. Trans R Soc Trop Med Hyg 1978, 72:188–191
5. Fisher-Hoch SP, Brammer LT, Trappier SG, Hutwagner LC, Farrar BB, Ruo SL, Brown BG, Hermann LM, Perez-Oronoz GI, Goldsmith CS, Hanes MA, McCormick JB: Pathogenic potential of filoviruses: role of geographic origin of primate host and virus strain. J Infect Dis 1992, 166:753–763
6. Jaax NK, Davis KJ, Geisbert TW, Vogel P, Jaax GP, Topper M, Jahrling PB: Lethal experimental infection of rhesus monkeys with Ebola-Zaire (Mayinga) virus by the oral and conjunctival route of exposure. Arch Pathol Lab Med 1996, 120:140–155
7. Geisbert TW, Pushko P, Anderson K, Smith J, Davis KJ, Jahrling PB: Evaluation in nonhuman primates of vaccines against Ebola virus. Emerg Infect Dis 2002, 8:503–507
8. Ryabchikova E, Kolesnikova L, Smolina M, Tkachev V, Pereboeva L, Baranova S, Grazhdantseva A, Rassadkin Y: Ebola virus infection in guinea pigs: presumable role of granulomatous inflammation in pathogenesis. Arch Virol 1996, 141:909–921
9. Bray M, Hatfill S, Hensley L, Huggins JW: Haematological, biochemical and coagulation changes in mice, guinea-pigs and monkeys infected with a mouse-adapted variant of Ebola Zaire virus. J Comp Pathol 2001, 125:243–253
10. Bray M, Davis K, Geisbert T, Schmaljohn C, Huggins J: A mouse model for evaluation of prophylaxis and therapy of Ebola hemorrhagic fever. J Infect Dis 1998, 178:651–661
11. Connolly BM, Steele KE, Davis KJ, Geisbert TW, Kell WM, Jaax NK, Jahrling PB: Pathogenesis of experimental Ebola virus infection in guinea pigs. J Infect Dis 1999, 179(Suppl 1):S203–S217
12. Murphy FA: Pathology of Ebola virus infection. Ebola Virus Haemorrhagic Fever. Edited by SR Pattyn. New York, Elsevier/North-Holland Biomedical Press, 1978, pp 43–60
13. Zaki SR, Goldsmith CS: Pathologic features of filovirus infections in humans. Curr Top Microbiol Immunol 1999, 235:97–116
14. Davis KJ, Anderson AO, Geisbert TW, Steele KE, Geisbert JB, Vogel P, Connolly BM, Huggins JW, Jahrling PB, Jaax NK: Pathology of experimental Ebola virus infection in African green monkeys. Arch Pathol Lab Med 1997, 121:805–819
15. Jahrling PB, Geisbert J, Swearengen JR, Jaax GP, Lewis T, Huggins JW, Schmidt JJ, LeDuc JW, Peters CJ: Passive immunization of Ebola virus-infected cynomolgus monkeys with immunoglobulin from hyperimmune horses. Arch Virol 1996, 11(Suppl):135–140
16. Jahrling PB, Geisbert TW, Geisbert JB, Swearengen JR, Bray M, Jaax NK, Huggins JW, LeDuc JW, Peters CJ: Evaluation of immune globulin and recombinant interferon-α2b for treatment of experimental Ebola virus infections. J Infect Dis 1999, 179(Suppl 1):S224–S234
17. Sullivan NJ, Sanchez A, Rollin PE, Yang Z-Y, Nabel GJ: Development of a preventative vaccine for Ebola virus infection in primates. Nature 2000, 408:605–609
18. Fisher-Hoch SP, Platt GS, Neild GH, Southee T, Baskerville A, Raymond RT, Lloyd G, Simpson DIH: Pathophysiology of shock and hemorrhage in a fulminating viral infection (Ebola). J Infect Dis 1985, 152:887–894
19. Johnson E, Jaax N, White J, Jahrling P: Lethal experimental infections in rhesus monkeys by aerosolized Ebola virus. Int J Exp Pathol 1995, 76:227–236
20. P'yankov OV, Sergeev AN, P'ankova OG, Chepurnov AA: Experimental Ebola fever in macaca rhesus. Vopr Virusol 1995, 40:113–115
21. Mikhailov VV, Borisevich IV, Chernikova NK, Potryvaeva NV, Krasnyanskii VP: An evaluation of the possibility of Ebola fever specific prophylaxis in baboons (Papio hamadryas). Vopr Virusol 1994, 39: 82–84
22. Borisevich IV, Mikhailov VV, Krasnyanskii VP, Gradoboev VN, Lebedinskaya YV, Potryvaeva NV, Timan'kova GD: Creation and study of immunoglobulin to Ebola fever. Vopr Virusol 1995, 40:270–273
23. Chepurnov AA, Chernukhin IV, Ternovoi VA, Kudoiarova NM, Makhova NM, Azaev MSh, Smolina MP: Attempts to develop a vaccine against Ebola fever. Vopr Virusol 1995, 40:257–260
24. Markin VA, Mikhailov VV, Krasnyanskii VP, Borisevich IV, Firsova IV: Development of emergency prophylaxis and treatment of Ebola fever. Vopr Virusol 1997, 42:31–34
25. Kudoyarova-Zubavichene NM, Sergeyev NN, Chepurnov AA, Netesov SV: Preparation and use of hyperimmune serum for prophylaxis and therapy of Ebola virus infections. J Infect Dis 1999, 179(Suppl 1):S218–S223
26. Ryabchikova EI, Kolesnikova LV, Luchko SV: An analysis of features of pathogenesis in two animal models of Ebola virus infection. J Infect Dis 1999, 179(Suppl 1):S199–S202
27. Prophet EB, Mills B, Arrington JB, Sobin LH: Laboratory Methods in Histotechnology. Washington DC, Armed Forces Institute of Pathology, 1992, pp 25–59
28. Geisbert TW, Hensley LE, Gibb TR, Steele KE, Jaax NK, Jahrling PB: Apoptosis induced in vitro and in vivo during infection by Ebola and Marburg viruses. Lab Invest 2000, 80:171–186
29. Jahrling PB: Filoviruses and Arenaviruses. Manual of Clinical Microbiology. Edited by PR Murray, EJ Baron, M Pfaller, FC Tenover, RH Yolken. Washington DC, ASM Press, 1999, pp 1125–1136
30. Hensley LE, Young HA, Jahrling PB, Geisbert TW: Proinflammatory response during Ebola virus infection of primate models: possible involvement of the tumor necrosis factor receptor superfamily. Immunol Lett 2002, 80:169–179
31. Soilleux EJ, Morris LS, Leslie G, Chehimi J, Luo Q, Levroney E, Trowsdale J, Montaner LJ, Doms RW, Weissman D, Coleman N, Lee B: Constitutive and induced expression of DC-SIGN on dendritic cell and macrophage subpopulations in situ and in vitro. J Leukoc Biol 2002, 41:445–457

32. Geisbert TW, Jahrling PB: Differentiation of filoviruses by electron microscopy. Virus Res 1995, 39:129–150
33. Moschella SL, Cropley TG: Mononuclear phagocytic and dendritic cell systems. J Am Acad Dermatol 1990, 22:1091–1097
34. Wacker HH, Radzun HJ, Parwaresch MR: Accessory cells in normal human and rodent lymph nodes: morphology, phenotype, and functional implications. Curr Top Pathol 1990, 84:193–218
35. Steele K, Crise B, Kuehne A, Kell W: Ebola virus glycoprotein demonstrates differential cellular localization in infected cell types of nonhuman primates and guinea pigs. Arch Pathol Lab Med 2001, 125:625–630
36. Majno G, Joris I: Apoptosis, oncosis, and necrosis: an overview of cell death. Am J Pathol 1995, 146:3–15
37. Granville DJ, Carthy CM, Hunt DWC, McManus BM: Apoptosis: molecular aspects of cell death and disease. Lab Invest 1998, 78:893–913
38. Ferrarini M, Grossi CE: Ultrastructure and cytochemistry of the human large granular lymphocytes. Immunobiology of Natural Killer Cells. Edited by E Lotzova, RB Herberman. Boca Raton, CRC Press, 1986, pp 34–50
39. Neighbour PA, Huberman HS, Kress Y: Human large granular lymphocytes and natural killing: ultrastuctural studies of strontium-induced degranulation. Eur J Immunol 1982, 588–595
40. Geisbert TW, Young HA, Jahrling PB, Davis KJ, Larsen T, Kagan E, Hensley LE: Pathogenesis of Ebola hemorrhagic fever in primate models: evidence that hemorrhage is not the direct effect of virus-induced cytolysis of endothelial cells. Am J Pathol 2003, 163:2371–2382
41. Geisbert TW, Jahrling PB, Hanes MA, Zack PM: Association of Ebola related Reston virus particles and antigen with tissue lesions of monkeys imported to the United States. J Comp Pathol 1992, 106:137–152
42. Baumann H, Gauldie J: The acute phase response. Immunol Today 1994, 15:74–89
43. Feldmann H, Bugany H, Mahner F, Klenk H-D, Drenckhahn D, Schnittler H-J: Filovirus-induced endothelial leakage triggered by infected monocytes/macrophages. J Virol 1996, 70:2208–2214
44. Stroher U, West E, Bugany H, Klenk HD, Schnittler HJ, Feldmann H: Infection and activation of monocytes by Marburg and Ebola viruses. J Virol 2001, 75:11025–11033
45. Banchereau J, Briere F, Caux C, Davoust J, Lebecque S, Liu YJ, Pulendran B, Palucka K: Immunobiology of dendritic cells. Annu Rev Immunol 2000, 18:767–811
46. Stingl G, Bergstresser PR: Dendritic cells: a major story unfolds. Immunol Today 1995, 16:330–333
47. Larsen CP, Steinman RM, Witmer-Pack M, Hankins DF, Morris PJ, Austyn JM: Migration and maturation of Langerhans cells in skin transplants and explants. J Exp Med 1990, 172:1483–1493
48. Inaba K, Metlay JP, Crowley MT, Steinman RM: Dendritic cells pulsed with protein antigens in vitro can prime antigen-specific, MHC-restricted T cells in situ. J Exp Med 1990, 172:631–640
49. Macatonia SE, Gompels M, Pinching AJ, Patterson S, Knight SC: Antigen-presentation by macrophages but not by dendritic cells in human immunodeficiency virus (HIV) infection. Immunology 1992, 75:576–581
50. Blauvelt A, Clerici M, Lucey DR, Streinberg SM, Yarchoan R, Walker R, Shearer GM, Katz SI: Functional studies of epidermal Langerhans cells and blood monocytes in HIV-infected persons. J Immunol 1995, 154:3506–3515
51. Grosjean I, Caux C, Bella C, Berger I, Wild F, Banchereau J, Kaiserlian D: Measles virus infects human dendritic cells and blocks their allostimulatory properties for $CD4^+$ T Cells. J Exp Med 1997, 186:801–812
52. Fugier-Vivier I, Servet-Delprat C, Rivailler P, Rissoan M-C, Liu Y-J, Rabourdin-Combe C: Measles virus suppresses cell-mediated immunity by interfering with the survival and function of dendritic and T cells. J Exp Med 1997, 186:813–823
53. Schnorr J-J, Xanthakos S, Keikavoussi P, Kampgen E, ter Meulen V, Schneider-Schaulies S: Induction of maturation of human blood dendritic cell precursors by measles virus is associated with immunosuppression. Proc Natl Acad Sci 1997, 94:5326–5331
54. Sevilla N, Kunz S, Holz A, Lewicki H, Homann D, Yamada H, Campbell KP, de la Torre JC, Oldstone MB: Immunosuppression and resultant viral persistence by specific viral targeting of dendritic cells. J Exp Med 2000, 192:1249–1260
55. Ho L-J, Wang J-J, Shaio M-F, Kao C-L, Chang D-H, Han S-W, Lai J-H: Infection of human dendritic cells by dengue viruses causes cell maturation and cytokine production. J Immunol 2001, 166:1499–1506
56. Raftery MJ, Schwab M, Eibert SM, Samstag Y, Walczak H, Schonrich G: Targeting the function of mature dendritic cells by human cytomegalovirus: a multilayered viral defense strategy. Immunity 2001, 15:997–1009
57. Kruse M, Rosorius O, Kratzer F, Stelz G, Kuhnt C, Schuler G, Hauber J, Steinkasserer A: Mature dendritic cells infected with herpes simplex virus type 1 exhibited inhibited T-cell stimulatory capacity. J Virol 2000, 74:7127–7136
58. Bukreyev A, Volchkov VE, Blinov VM, Netesov SV: The GP-protein of Marburg virus contains the region similar to the 'immunosuppressive domain' of oncogenic retrovirus P15E proteins. FEBS Lett 1993, 323:183–187
59. Sanchez A, Kiley MP, Holloway BP, Auperin DD: Sequence analysis of the Ebola virus genome: organization, genetic elements, and comparison with the genome of Marburg virus. Virus Res 1993, 29:215–240
60. Sanchez A, Trappier SG, Mahy BW, Peters CJ, Nichol ST: The virion glycoproteins of Ebola viruses are encoded in two reading frames and are exposed through transcriptional editing. Proc Natl Acad Sci USA 1996, 93:3602–3607
61. Baize S, Leroy EM, Georges-Courbot M-C, Capron M, Lansoud-Soukate J, Debre P, Fisher-Hoch SP, McCormick JB, Georges AJ: Defective humoral responses and extensive intravascular apoptosis are associated with fatal outcome in Ebola virus-infected patients. Nat Med 1999, 5:423–426
62. Baize S, Leroy EM, Mavoungou E, Fisher-Hoch SP: Apoptosis in fatal Ebola infection. Does the virus toll the bell for immune system? Apoptosis 2000, 5:5–7
63. Andrade F, Bull HG, Thornberry NA, Ketner GW, Casciola-Rosen LA, Rosen A: Adenovirus L4–100K assembly protein is a granzyme B substrate that potently inhibits granzyme B-mediated cell death. Immunity 2001, 14:751–761
64. Kayagaki N, Yamaguchi N, Nakayama M, Eto H, Okumura K, Yagita H: Type I interferons (IFNs) regulate tumor necrosis factor-related apoptosis-inducing ligand (TRAIL) expression on human T cells: a novel mechanism for the antitumor effects of type I INFs. J Exp Med 1999, 189:1451–1460
65. Dhib-Jalbut SS, Cowan EP: Direct evidence that interferon-beta mediates enhanced HLA-class I expression in measles virus-infected cells. J Immunol 1993, 151:6248–6258
66. Griffith TS, Wiley SR, Kubin MZ, Sedger LM, Maliszewski CR, Fanger NA: Monocyte-mediated tumoricidal activity via the tumor necrosis factor-related cytokine, TRAIL. J Exp Med 1999, 189:1343–1353
67. Vidalain P-O, Azocar O, Lamouille B, Astier A, Rabourdin-Combe C, Servet-Delpart C: Measles virus induces functional TRAIL production by human dendritic cells. J Virol 2000, 74:556–559
68. Beaulieu S, Lafontaine M, Richer M, Courchesne I, Cohen EA, Bergeron D: Characterization of the cytotoxic factor(s) released from thymic dendritic cells upon human immunodeficiency virus type 1 infection. Virology 1998, 241:285–297
69. Katsikis PD, Garcia-Ojeda ME, Torres-Roca JF, Tijoe IM, Smith CA, Herzenberg LA, Herzenberg LA: Interleukin-1 β converting enzyme-like protease involvement in Fas-induced and activation-induced peripheral blood T cell apoptosis in HIV infection: TNF-related apoptosis-inducing ligand can mediate activation-induced T cell death in HIV infection. J Exp Med 1997, 186:1365–1372
70. Jeremias I, Herr I, Boehler T, Debatin KM: TRAIL/Apo-2-ligand-induced apoptosis in human T cells. Eur J Immunol 1998, 28:143–152
71. Pavlovic J, Arzet HA, Hefti HP, Frese M, Rost D, Ernst B, Kolb E, Staeheli P, Haller O: Enhanced virus resistance of transgenic mice expressing the human MxA protein. J Virol 1995, 69:4506–4510
72. Cella M, Salio M, Sakakibara Y, Langen H, Julkunen I, Lanzavecchia A: Maturation, activation, and protection of dendritic cells induced by double-stranded RNA. J Exp Med 1999, 189:821–829
73. Wong BR, Josien R, Lee SY, Sauter B, Li HL, Steinman RM, Choi Y: TRANCE (tumor necrosis factor [TNF]-related activation-induced cytokine), a new TNF family member predominantly expressed in T

cells, is a dendritic cell-specific survival factor. J Exp Med 1997, 186:2075–2080
74. Yeh WC, Shahinian A, Speiser D, Kraunus J, Billia F, Wakeham A, de la Pompa JL, Ferrick D, Hum B, Iscove N, Ohashi P, Rothe M, Goeddel DV, Mak TW: Early lethality, functional NF-κB activation, and increased sensitivity to TNF-induced cell death in TRAF2-deficient mice. Immunity 1997, 7:715–725
75. Takabayashi A, Kawai Y, Iwata S, Kanai M, Denno R, Kawada K, Obama K, Taki Y: Nitric oxide induces a decrease in the mitochondrial membrane potential of peripheral blood lymphocytes, especially in natural killer cells. Antioxid Redox Signal 2000, 2:673–680
76. Villinger F, Rollin PE, Brar SS, Chikkala NF, Winter J, Sundstrom JB, Zaki SR, Swanepoel R, Ansari AA, Peters CJ: Markedly elevated levels of interferon (IFN)-α, IFN-γ, interleukin (IL)-2, IL-10, and tumor necrosis factor-α associated with fatal Ebola virus infection. J Infect Dis 1999, 179(Suppl 1):S188–S191
77. Bailly S, Fay M, Gougerot-Pocidalo MA: Effects of antibiotics on production of cytokines by human monocytes. Pathol Biol (Paris) 1993, 41:838–844
78. Morikawa K, Watabe H, Araake M, Morikawa S: Modulatory effect of antibiotics on cytokine production by human monocytes in vitro. Antimicrob Agents Chemother 1996, 40:1366–1370
79. van Vlem B, Vanholder R, de Paepe P, Vogelaers D, Ringoir S: Immunomodulating effects of antibiotics: a literature review. Infection 1996, 24:275–291
80. Khan AA, Slifer TR, Araujo FG, Remington JS: Effect of clarithromycin and azithromycin on production of cytokines by human monocytes. Int J Antimicrob Agents 1999, 11:121–132
81. Guo W, Ding J, Huang Q, Jerrels T, Deitch EA: Alterations in intestinal bacterial flora modulate the systemic cytokine response to hemorrhagic shock. Am J Physiol 1995, 269:G827–G832
82. Guo W, Magnotti LJ, Ding J, Huang Q, Xu D, Deitch EA: Influence of gut microflora on mesenteric lymph cytokine production in rats with hemorrhagic shock. J Trauma 2002, 52:1178–1185